ACS NANO

www.acsnano.org

Article

Remotely Tuned Triplet Transfer via Ligand Proximity in Quantum Dot–Organic Spectral Converters

Yanhong Fan,[#] Jia Luo,[#] Ziqi Wang,[#] Yanchao Zhao, Shuangke Wu, Yuqi Sun, Peng Zhang, Haoyu Song, Xianggui Zhou, Zhiqiang Hu, Jiajie Wu, Yaqi Gu, Lu Qiu, Zhuang Miao, Sanyang Han, Xing Jiang, Victor Gray, Jiajia Zhou, Akshay Rao,* and Zhilong Zhang*

Cite This: https://doi.org/10.1021/acsnano.5c22144

Read Online

ACCESS | Metrics & More | Article Recommendations | Supporting Information

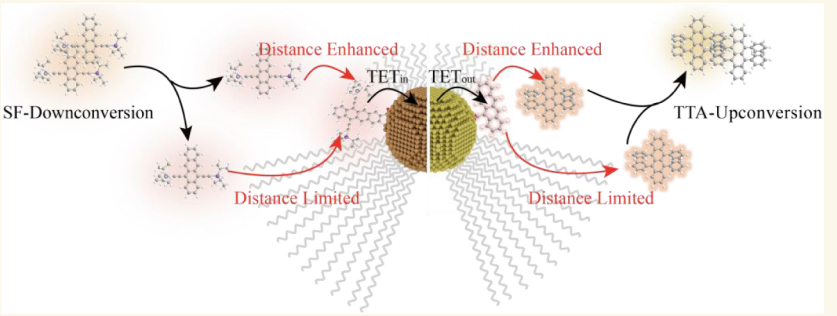

ABSTRACT: Quantum dot (QD)–organic hybrid materials offer promising spectral conversion platforms for applications such as photoredox catalysis, solar energy conversion, 3D printing, and bioimaging. In spectral upconversion, the overall triplet energy transfer (TET) efficiency remains limited due to inefficient secondary TET that occurs beyond the QD core, i.e., from triplet mediators to annihilators (TET2). Here, we reveal that the hydrocarbon ligands on nanoparticles can remotely govern this external TET2 that occurs entirely outside the core. By shrinking the native oleate ligand shell on PbSe QD sensitizers before attaching triplet mediator ligands, the NIR-to-visible upconversion performance can be significantly improved. Transient absorption spectroscopy confirms that the more compact ligand shell substantially accelerates TET2, boosting the highest transfer efficiency from 59.4% to 93.5%. We propose that the enhanced TET2 stems from shortened mediator-annihilator distances induced by reduced steric hindrance from the shorter, proximal hydrocarbon ligands, as confirmed by molecular dynamics simulations. The strategy proves versatile across multiple upconversion systems, including solid-state films, CdSe QD-based green-to-blue systems, and lanthanide-doped nanoparticle-sensitized hybrids. Furthermore, the same principle remains applicable to molecular singlet fission–based downconversion using QD as photon emitters, raising the highest photon–multiplication efficiency from 132% to 163%. Our work demonstrates that ligand shell proximity can remotely tune TET beyond the nanoparticle core, providing a general route to optimize inorganic–organic hybrid spectral up- and downconverters.

KEYWORDS: *triplet energy transfer, upconversion, triplet–triplet annihilation, singlet fission, downconversion, quantum dots, lanthanides*

INTRODUCTION

Colloidal quantum dots (QDs) have emerged as a new class of triplet sensitizers and acceptors for organic molecules, thanks to their tunable bandgaps, high extinction coefficients, high triplet exciton generation yields, and exceptional photostability. When coupled with organic molecules, they can enable the generation of molecular triplet excitons that cannot be directly excited by photons through efficient Dexter energy transfer, eliminating the need for intersystem crossing.[1−6] Sensitized molecular triplet excitons are key to triplet–triplet-annihilation-based photon upconversion (TTA-UC), the process that converts low-energy light into higher-energy emission. Conversely, when paired with singlet-fission (SF) chromophores, QDs can accept the generated triplets and re-emit them as multiple lower-energy photons, yielding photon multiplicative downconversion (SF-DC).[7−10] Such spectral conversion platforms have emerged as important technologies with broad applications in photocatalysis,[11,12] bioimaging,[13,14] 3D printing,[15] and solar energy harvesting.[6,16−19]

In TTA-UC, these material systems rely on triplet energy transfer (TET) among three key components: the QD sensitizer, a mediator ligand, and an annihilator molecule.

Received: December 18, 2025
Revised: March 6, 2026
Accepted: March 6, 2026

Recent advances in mediator ligands anchored to QD surfaces enable them to bridge the QD core and solution-phase annihilators, overcoming TET inhibition induced by the long aliphatic ligand shell. Their long triplet lifetimes also exceed the self-recombination lifetimes of QD excitons, extending the exciton lifetime window to facilitate subsequent TET to annihilators.[20−23] However, currently, the overall transfer efficiency is still limited. Upon photoexcitation, the excitons generated in a QD are extracted through a two-step energy transfer (Scheme 1): (1) the TET from the QD core to the mediator ligand directly bound to its surface (TET1), and (2) the secondary TET outside the QD core, from the mediator ligand to the annihilator (TET2), followed by the generation of upconverted photons through TTA. The overall TET efficiency is determined by the product of the efficiencies for both transfer processes ($\Phi_{TET} = \Phi_{TET1} \times \Phi_{TET2}$). To date, the efficiency of TET1 has been improved to over 90% in many material combinations, owing to strategies such as QD shell engineering,[24−26] doping,[27,28] passivation,[29] stoichiometry control,[11,30] wave function control of QDs,[31,34] energetics control of the transfer processes,[35,36] and the design of new mediator ligands.[37] However, the efficiency of the equally critical TET2 process remains relatively low (typically 40−60%)[38,39] due to the lack of effective improvement strategies, which limits the overall TET efficiency and further development in TTA-UC. It has been demonstrated that TET2 can be improved by extending the mediators' anchoring group to QDs (as the mediator-annihilator distance is reduced), but this is at the cost of inhibiting TET1 as the QD-mediator distance is also concomitantly increased. Currently, the only rational strategy to improve TET2 is to increase the triplet lifetime of the mediator,[39] which would require redesigning the molecular structures of all mediators working in different wavelength ranges, making it challenging in practice. A universal strategy that can enhance TET2 without inhibiting TET1, while being applicable across all upconversion wavelength ranges, is therefore needed in order to overcome the current limitations on TET in QD-organic hybrid materials.

Here, we report the discovery that modifications of the hydrocarbon ligand shell on QDs can indeed remotely tune the TET2 process, even though the QD is not directly involved in this step, thereby overcoming the current bottlenecks of TET in QD-organic hybrid upconverters. Aliphatic hydrocarbon ligands such as oleates (OA) are commonly used in the synthesis of QDs, and they serve as passivation sources as well as stabilizers that keep QDs dispersible in solution. It has been extensively reported that these hydrocarbon ligands have a major impact on direct energy/charge transfer between the QD core and nearby donors/acceptors.[1,23,40,41] We propose that these hydrocarbon ligands can have an even more significant impact on TET2, despite the QD core playing no direct role in this process. When forming a QD-organic mediator triplet sensitizer system, these hydrocarbon ligands are only partially replaced by the mediator ligands,[11,24] while a decent amount of them still remain to maintain the colloidal stability of QDs. These two species of ligands together form the ligand proximity on the surface of QDs (Scheme 1). By reducing the length of the hydrocarbon ligands, we demonstrate that the upconversion QY of the system can be substantially improved. Through a series of photophysical characterizations of the TET dynamics, we confirm that the TET2 transfer rate from the mediator to the annihilator is significantly enhanced, increasing the transfer efficiency from 59.4% to 93.5%, which surpasses those reported previously.[38,39] Our molecular dynamics simulations show that the enhancements likely arise from the shortened mediator-annihilator distance induced by the reduced steric hindrance from the shorter, proximal hydrocarbon ligands. Efficient TET1 is also retained with this strategy. We further examine the versatility of the proposed strategy and found it to be generally effective across multiple upconversion systems, including solid-state films, CdSe QD-based green-to-blue systems, and even lanthanide nanoparticle-sensitized hybrids. Furthermore, the same principle remains applicable to molecular SF-DC using QDs as photon emitters, significantly improving the photon-multiplication efficiency from 132% to 163%. We propose that fine-tuning the surface ligand proximity of nanoparticles can be an effective route to break the current bottleneck of the overall TET efficiency in various spectral conversion systems.

Scheme 1. Schematic of Triplet Energy Transfer in QD-Organic Upconversion Hybrids[ab]

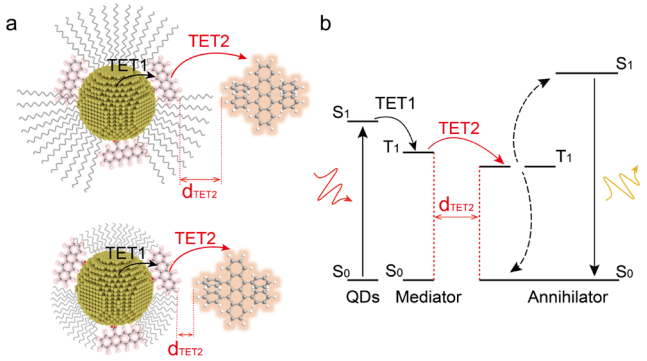

[a]Upon photoexcitation, the excitons generated in QDs first transfer to the mediator ligands (TET1), followed by the secondary transfer to the annihilator molecules (TET2). The TET2 process can be largely affected by the distance between the mediator and annihilator, which depends on the compactness of the hydrocarbon ligands of the QDs. [b]Energy transfer diagram of the QD-organic upconversion hybrids.

RESULTS AND DISCUSSION

An upconversion hybrid comprising lead selenide (PbSe) QDs, 5-carboxylic acid tetracene (5CT) mediator ligands, and rubrene annihilators was employed in this work. PbSe QDs were synthesized and employed as the triplet sensitizer owing to their suitable band gap in the near-infrared (NIR) region and relatively large exciton Bohr radius, which is considered to be favorable for triplet energy transfer.[31,32] We used the well-established hot injection method by mixing lead oleate and trioctylphosphine selenide (see Experimental Methods Section for details) at elevated temperatures. Monodispersed QDs with an excitonic peak at ∼840 nm (corresponding to a band gap of ∼1.47 eV) were obtained. The QDs were capped by OA ligands, originating from oleic acid introduced during the synthesis. While OA ligands provide adequate surface passivation and colloidal stability to the QDs, the 18 carbon atoms in their hydrocarbon chains are known to hinder charge and energy transfer between the QDs and other materials.[23,42−44] We hypothesize that the OA ligands not only impede direct triplet energy transfer from the QDs to annihilator molecules but also limit the efficiency of TET2, as the overall ligand shell might maintain a relatively large

https://doi.org/10.1021/acsnano.5c22144
ACS Nano XXXX, XXX, XXX−XXX

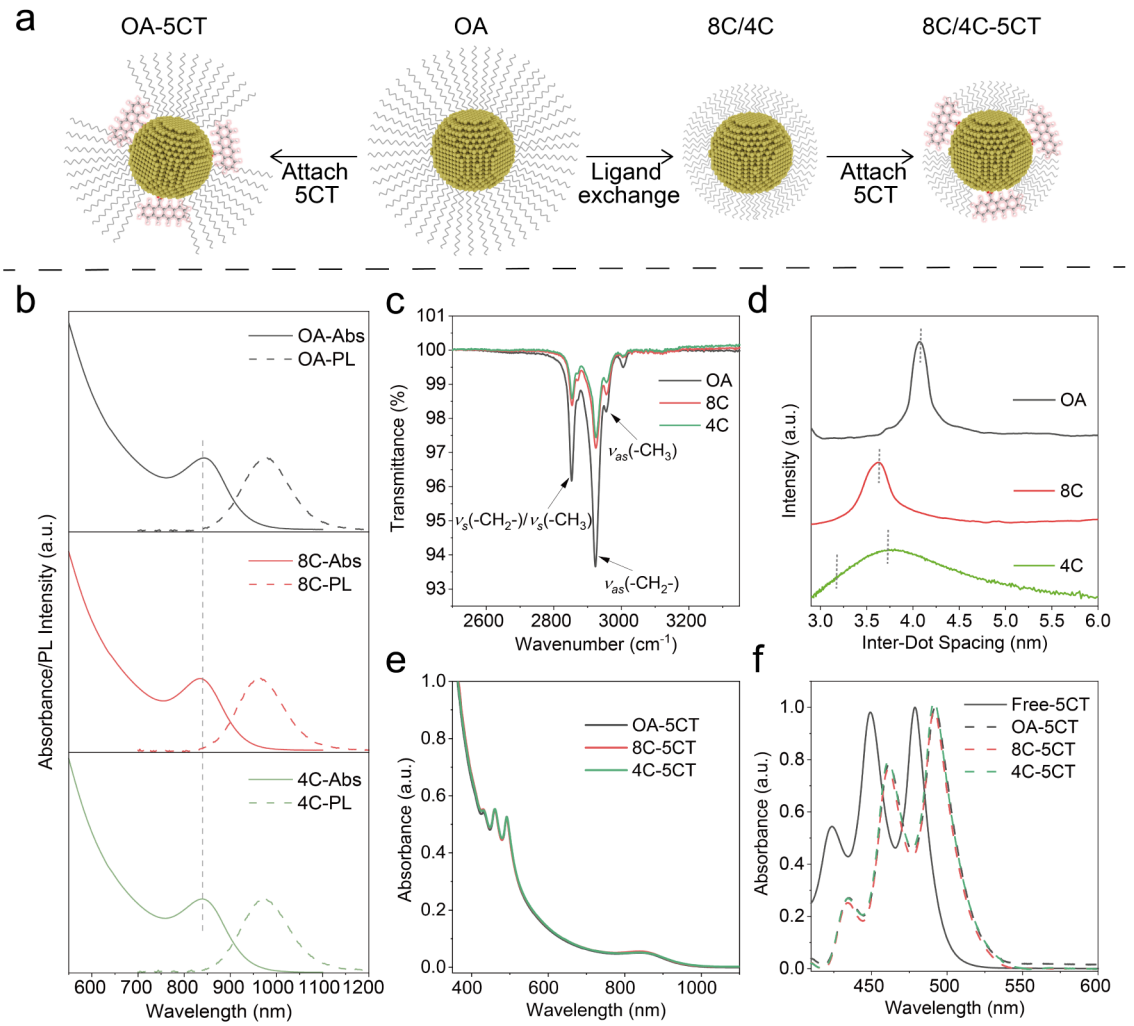

Figure 1. Ligand exchange of the QDs and characterizations. (a) Schematic of the ligand exchange processes and attachment to 5CT mediator ligands. (b) UV−vis absorption (solid lines) and photoluminescence (dashed lines) spectra of PbSe QDs capped with OA, 8C, and 4C ligands. (c) FTIR spectra of the QDs with different ligands; the corresponding vibration modes are labeled. (d) Interdot spacing of QD thin films with different surface ligands, derived from SAXS results. (e) UV−vis absorption of the QDs after attachment of 5CT mediator ligands; clear 5CT absorption features can be observed at 400−500 nm. (f) Comparison between the absorption spectra of free 5CT molecules (black solid line) and those bonded to PbSe QDs (dashed lines, obtained by subtracting the QD-only spectra from those after attachment of 5CT). The red shifts of the bound 5CT ligands indicate electronic coupling with QDs.

distance between the mediator ligand and the annihilator (Scheme 1). To facilitate closer contact between the mediator and annihilator ligands, we exchanged the OA ligands on the QDs with shorter hydrocarbon ligands, specifically octanoate (8C) or butyrate (4C), before attaching 5CT as the mediator ligands (Figure 1a). We observe negligible changes in both the amplitude and shape of the absorption and photoluminescence (PL) spectra of the QDs (Figure 1b), suggesting that the QD cores are well preserved after the ligand exchange treatments. This is further supported by X-ray diffraction (XRD) patterns and transmission electron microscopy (TEM) images, which revealed no significant changes in the crystallinity and the monodispersed morphology of the QDs (Figures S1-S2 in the Supporting Information). Additionally, the photoluminescence quantum yield (PLQY) and the PL decay kinetics are similar for all QDs with OA, 8C, or 4C ligands (Tables S2-S3 and Figure S7), implying that the ligand exchange did not create noticeable surface defects on the QDs.[45]

Fourier transform infrared (FTIR) spectroscopy revealed suppressed peaks at 2957, 2926, and 2854 cm^{-1}, corresponding to the $-CH_3$ asymmetric stretch, $-CH_2-$ asymmetric stretch, and $-CH_2-/-CH_3$ symmetric stretch, respectively (Figure 1c). This confirms successful ligand exchange from the long-chain OA to the shorter ligands.[46−49] Thermogravimetric analysis (TGA) also showed a lower contribution of the ligands to the total mass of QDs when the OA ligands were replaced with 8C or 4C ligands (Figure S3). This also implies successful ligand exchange, as the ligands bonded to the QDs now are lighter.[49,50] We also performed ^{1}H nuclear magnetic resonance (NMR) measurements on the QDs (Figure S4). By quantifying the amount of hydrogen protons bonded to the carbon−carbon double bond, which is unique for OA ligands, we found that more than 90% of OA ligands are replaced with the shorter ligands (Table S1). To elucidate the change in ligand shell compactness, we fabricated QD thin films (with different ligands) and carried out small-angle X-ray scattering (SAXS) measurements to reveal the interdot distance. It has been well demonstrated that the interdot distance is mainly dominated by the thickness of the ligand shell, which is essentially determined by the ligand length.[40,45,51] From the

https://doi.org/10.1021/acsnano.5c22144
ACS Nano XXXX, XXX, XXX−XXX

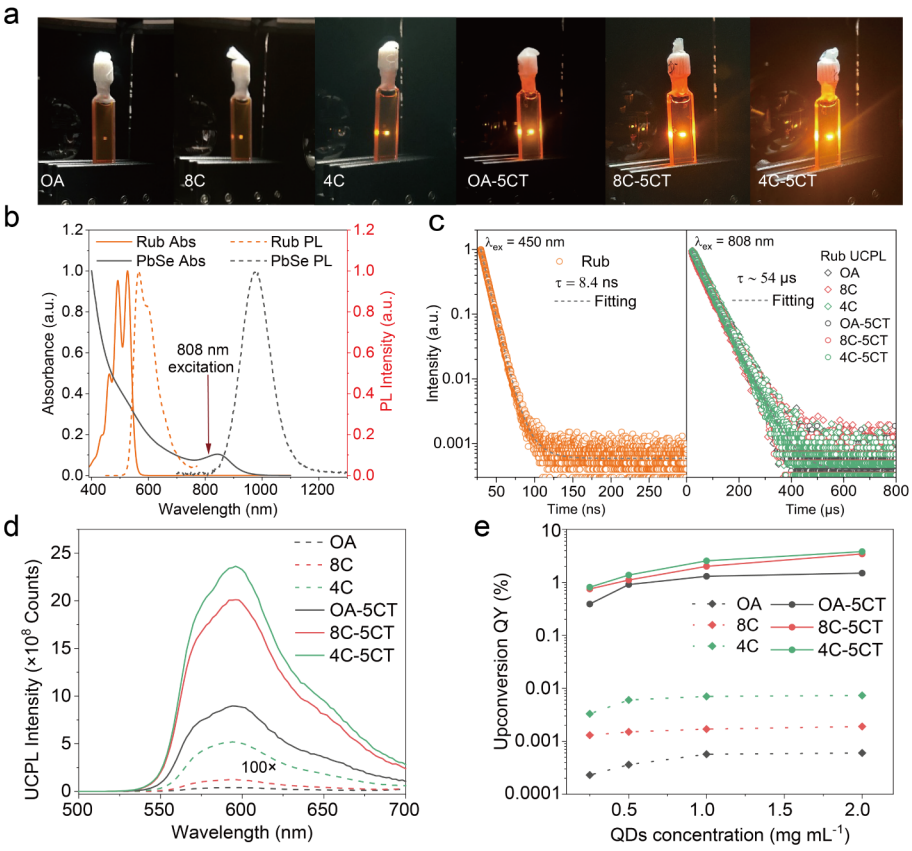

Figure 2. Upconversion emission and performance of the QD-organic hybrids. (a) Photograph of the NIR-to-yellow upconversion emission from samples with QDs possessing different surface ligands; the samples were placed in 1 mm quartz cuvettes and excited using an 808 nm continuous-wave laser. (b) Absorption (solid lines) and emission (dashed lines) spectra of rubrene and PbSe QDs taken in toluene at room temperature; the 808 nm excitation is absorbed only by the QDs. (c) Time-resolved PL decay of rubrene under 450 nm (direct) and 808 nm (indirect) excitation; the extended lifetimes with 808 nm can be attributed to the upconversion processes involving long-lived triplet excitons. The fitting was produced from OA-5CT. (d) Relative upconversion PL spectra of samples with QDs possessing different ligand proximities; those without 5CT mediators are scaled up by 100. (e) Upconversion QYs of the samples at different QD concentrations; shorter hydrocarbon ligands always lead to higher QYs regardless of whether 5CT mediators are attached.

azimuthal integration of the diffraction patterns, we calculated the interdot spacing in the QD films (Figure 1d and Figure S5). For OA-capped QDs, the interdot distance in the film was approximately 4.2 nm, and it is reduced to 3.6 nm for 8C-capped QDs, indicating a more compact ligand shell. We noticed the QD film with 4C ligands showed a wider distribution of interdot distances, which spans over 3.1−5 nm, with an average distance of 3.7 nm. Such patterns have been reported previously. It can be attributed to less homogeneous packing of QDs, which is common in QD films with short ligands, causing regions with both long and short interdot distances in the same film (Figure S6).[40,51] As the average interdot distance with 4C is shorter than that with OA, and a large portion of the 4C-capped QDs possess the shortest interdot distance (down to ~3.1 nm) among all samples, we suggest that the ligand shell is effectively thinner than those with OA and 8C. We also note that the diameter of our QDs is approximately 2.7 nm; together with the interdot distances, we can calculate the ligand shell thickness. They are estimated to be 1.5, 0.9, and 0.4 nm for OA-, 8C-, and 4C-capped QDs, which are consistent with the ligand lengths reported previously,[52] confirming the successful modification of the ligand shell.

After attaching the 5CT mediator ligands and performing extensive purification, additional absorption peak features around 400−550 nm were observed in the QDs with different ligands (referred to as OA-5CT, 8C-5CT, and 4C-5CT in the following) (Figure 1e). These peaks are attributed to the absorption of 5CT bonded to the QDs. By subtracting the absorption spectra of pristine QDs from those of the 5CT-bonded QDs, clear redshifts in the 5CT peaks were observed. This redshift is likely due to energy coupling between 5CT and the QDs upon chemical bonding, or the change in the ligand's dielectric environment, as previously reported by other groups.[24, 53]Nevertheless, both cases would indicate successful incorporation of 5CT on the surface of the QDs. The coverage of 5CT was found to be approximately 12 ligands per dot, similar to that from other reports (see Experimental Methods Section for more details).[24,38] From the above results, we conclude that the ligand exchange from OA to shorter ligands was successful and had a negligible effect on the subsequent attachment of 5CT to the QDs.

Upconversion hybrid materials were then constructed by mixing the QDs with rubrene, which serves as both an annihilator and an emitter. We selected 5CT-rubrene as the mediator-rubrene combination because they have been well-verified for upconversion by many other groups.[4,39] Upon excitation with an 808 nm NIR laser, all samples exhibited visible PL (Figure 2a and Figure S9). Given that the QDs are the only component in the hybrids capable of being directly

https://doi.org/10.1021/acsnano.5c22144
ACS Nano XXXX, XXX, XXX−XXX

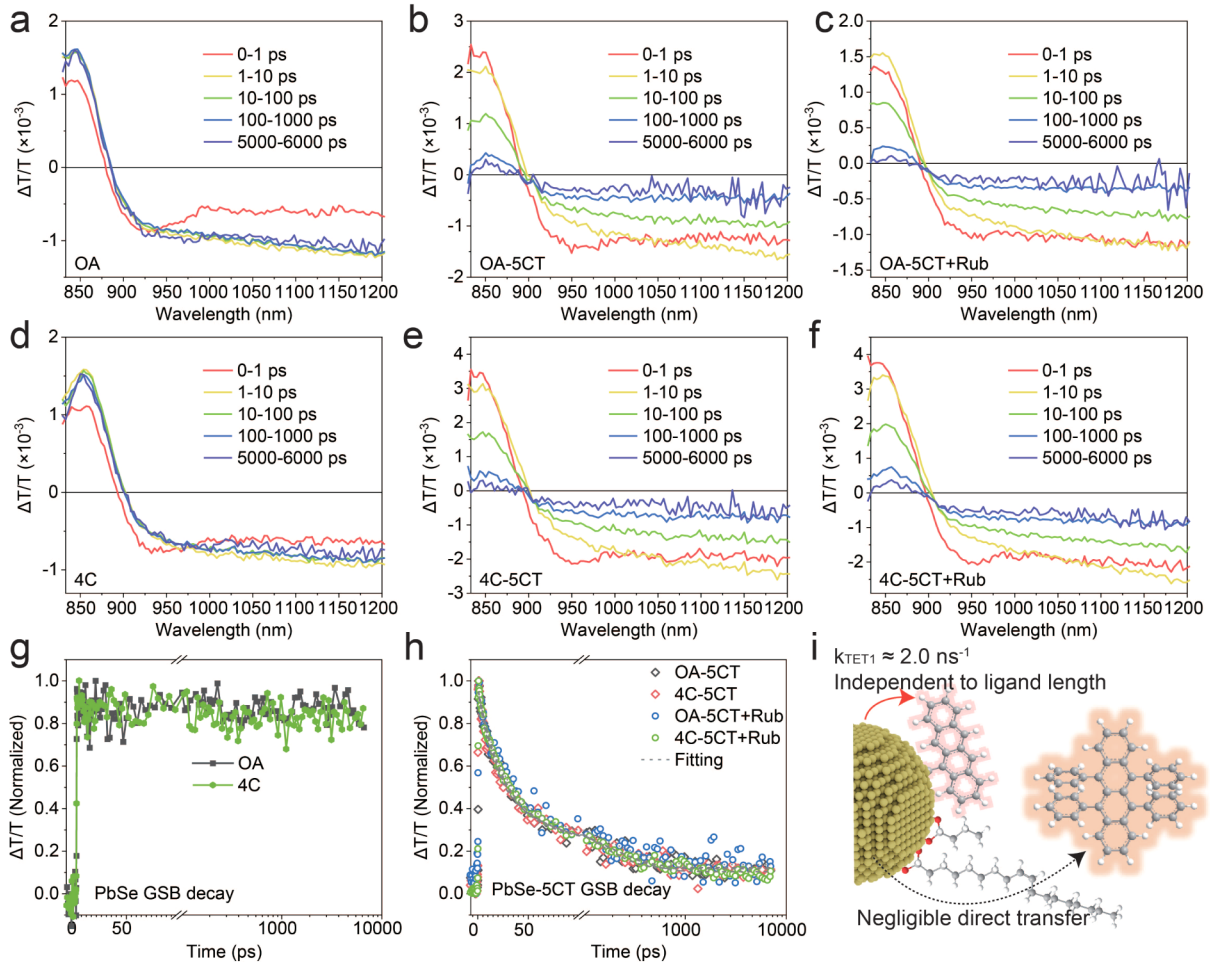

Figure 3. fs-TA spectra in the NIR range and decay kinetics of excitons in QDs. (a–c) TA spectra of QDs with OA, OA-5CT, and OA-5CT mixed with rubrene annihilators (Rub), respectively. (d–f) TA spectra of QDs with 4C, 4C-5CT, and 4C-5CT mixed with Rub annihilators, respectively. (g) Kinetics of ground-state bleach (GSB) at 840–900 nm representing exciton populations in QDs capped with OA or 4C; there is negligible decay within the time window (7.6 ns) measured. (h) Kinetics of GSB of QDs capped with OA-5CT or 4C-5CT before and after mixing with rubrene annihilators; the decay kinetics are all similar. The fitting was produced from OA-5CT. (i) Schematic illustration of the unchanged TET1 process and negligible direct transfer from QDs to annihilators.

excited by the 808 nm laser (Figure 2b), the observed yellow visible PL is attributed to the upconversion process, as depicted in Scheme 1. This is further supported by the PL decay kinetics. When rubrene is excited directly by a 450 nm laser, the PL lifetime is approximately 8.4 ns, while it extends to about 54 μs when the hybrid materials are excited by the 808 nm laser (Figure 2c and Figure S10). Such long PL lifetimes are indicative of the long-lived triplet excitons in rubrene before the TTA process (Table S4).[6,37] We observed that the upconversion intensity increases with shorter hydrocarbon ligands, regardless of whether the 5CT mediator ligands are attached (Figure 2a,d). The upconversion QY for the sample with OA-capped QDs is about 0.0006% (normalized to 100%), consistent with previous reports,[32] and it increased to 0.0019%, 0.0073% for QDs capped by 8C and 4C ligands, respectively, under optimized QD concentration (Figure 2e and Table S6). This trend is expected and consistent with previous reports,[23,54] which can be attributed to improved direct transfer from the QDs to rubrene annihilators when the hydrocarbon ligands are shorter, although the overall efficiencies are still minor (Table S6 and Note in the Supporting Information). Upon attaching the 5CT mediator ligands, the upconversion intensity significantly increases, as expected (Figure 2d).[32,33] The highest upconversion QY achieved for OA-5CT, 8C-5CT, and 4C-5CT are 1.49%, 3.43%, and 3.80%, respectively (Figure 2e and Table S6). This suggests that shorter hydrocarbon ligands can further enhance the upconversion performance even in the presence of the 5CT mediator ligands. We found that 4C-5CT consistently demonstrated higher upconversion QY than others when the concentration of 5CT or rubrene was modified (Figure S12). This is further supported by the power-dependent upconversion intensity measurements, which show a quadratic-to-linear transition at lower incident powers when the hydrocarbon ligands are shorter (Figure S13). We note that the highest upconversion QY reported here is lower than those reported by some other groups, which is likely caused by the higher QD loading ratio in this study.[11,38,53,55,56] To maintain more accurate QY measurements, we kept the QD concentration at 0.25–2 mg mL^{-1} (Figure 2e), corresponding to approximately 10% absorption of NIR laser excitation. These concentrations are higher than those reported by other groups;[38,56] therefore, the upconversion photon outcoupling efficiency might be lower due to more substantial reabsorption by the QDs, eventually causing lower average QY. We clarify that a higher absorption ratio in an upconversion system should be more

https://doi.org/10.1021/acsnano.5c22144
ACS Nano XXXX, XXX, XXX–XXX

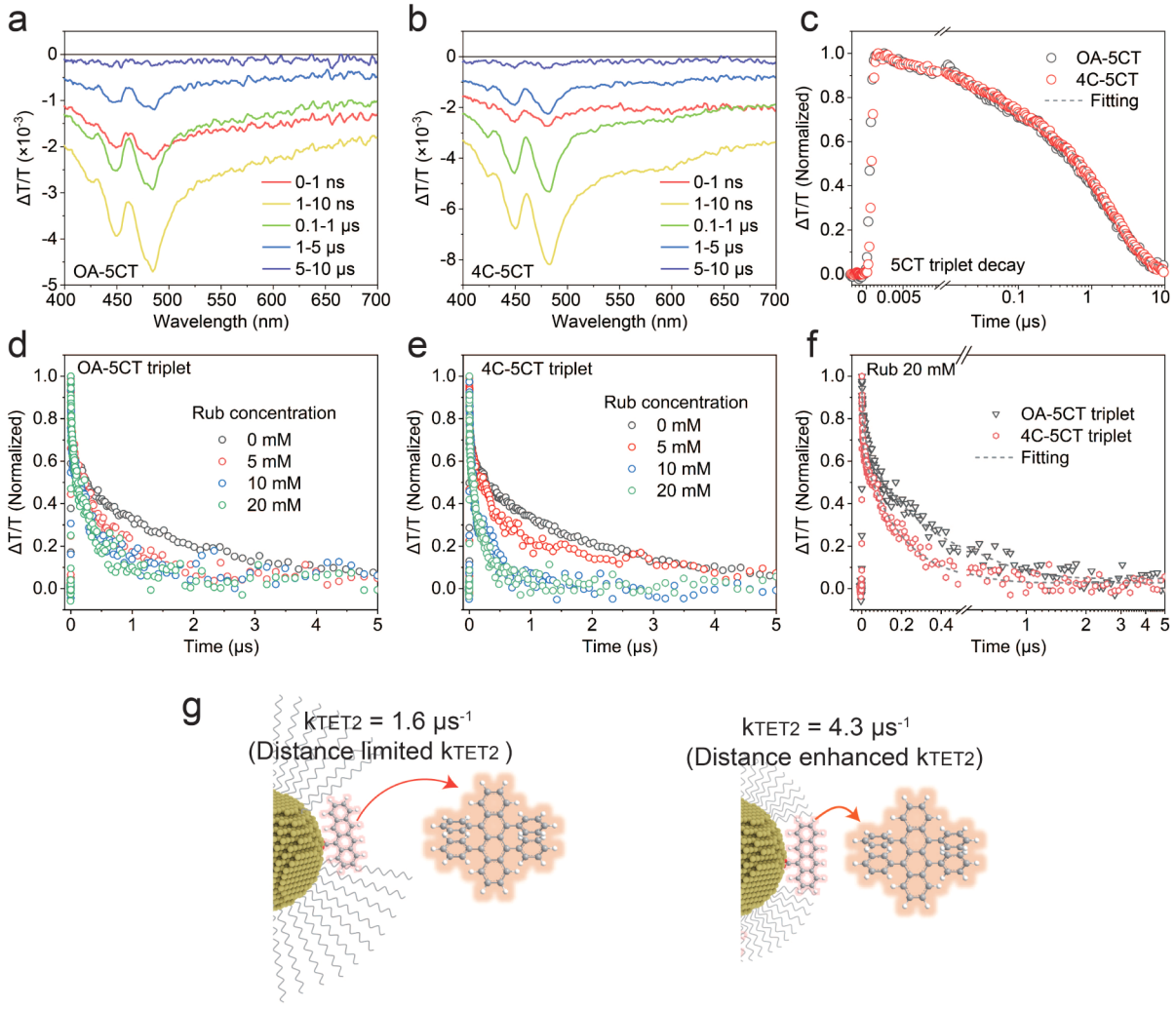

Figure 4. ns-TA in the visible range and analysis on TET2. TA spectra of QDs with (a) OA-5CT and (b) 4C-5CT ligand proximities. (c) Normalized kinetics of the PIA features (560−700 nm) representing triplet populations in the 5CT mediators; the decay kinetics are similar in both OA-5CT and 4C-5CT. Normalized kinetics of 5CT triplet population decay for QDs with (d) OA-5CT and (e) 4C-5CT ligand proximities when they are mixed with rubrene annihilators at different concentrations. (f) Comparison of the 5CT triplet kinetics in the presence of 20 mM rubrene; the faster decay in 4C-5CT indicates faster TET2. (g) Schematic illustration of the TET2 process with OA-5CT and 4C-5CT proximities; the transfer rate constants are indicated.

realistic in practical applications, and it should reduce the error when measuring QY (see Figure S8, Table S7 and discussion in the Supporting Information). Our samples were strictly prepared with the same standard; hence, the upconversion QY reported for each sample here should precisely reflect the corresponding energy transfer mechanisms. In addition, we found that the shorter hydrocarbon ligands do not cause noticeable changes in the stability of the upconversion system (Figure S14), further indicating that the improvement in upconversion performance arises from the more efficient TET processes.

Important questions arise regarding the underlying mechanisms that dictate the improved overall TET. We suggest that, in the absence of 5CT, although shorter hydrocarbon ligands can increase the upconversion QY by 1 order of magnitude (from 0.0006% to 0.0073%), the absolute improvement in efficiency remains minor (0.0067%), implying that the overall direct TET from QDs to the rubrene annihilator remains inefficient. On the other hand, with the 5CT mediator ligand, the highest upconversion QY is improved from 1.49% (OA-5CT) to 3.80% (4C-5CT). Such a significant enhancement in the absolute QY (2.31%) cannot be solely attributed to the slight enhancement of the direct TET from QDs to rubrene. Therefore, we suggest that the shorter hydrocarbon ligands should have improved the TET process where 5CT is involved, i.e., either TET1 or TET2 (Scheme 1).

To elucidate the impact of shorter hydrocarbon ligands on the TET within the hybrid materials, we employed femtosecond transient absorption (fs-TA) spectroscopy to investigate the underlying photophysical processes. We first examined the TA features in the NIR range to investigate the exciton transfer dynamics from the PbSe QDs. Pronounced photobleaching peak features (positive change in transmission, $\Delta T/T$) can be observed at approximately 840 nm in QDs with either OA or 4C ligands (Figure 3a and d), in good agreement with the first excitonic peak position of the QDs (Figure 1b).[40,57,58] Within the measurement time window of 7.6 ns, no significant decay was detected in the photobleaching signal of the QDs (Figure 3g), consistent with the relatively long exciton lifetimes (~2 μs) obtained from time-resolved PL

https://doi.org/10.1021/acsnano.5c22144
ACS Nano XXXX, XXX, XXX−XXX

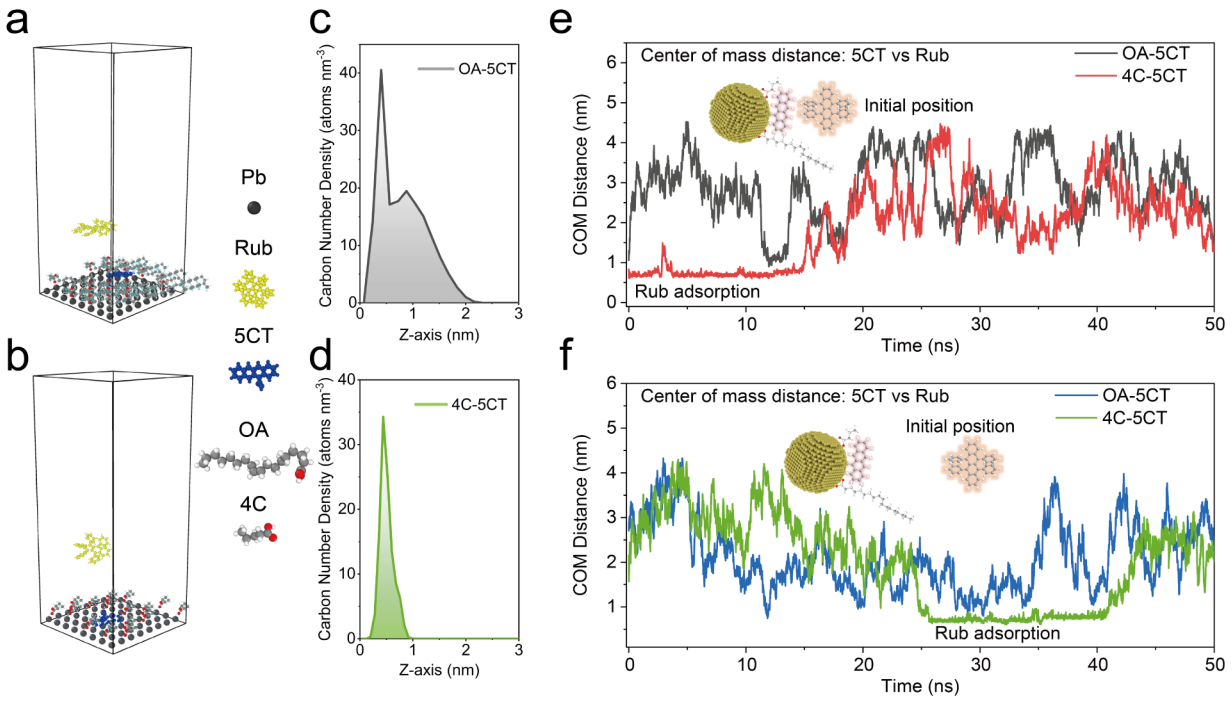

Figure 5. Molecular dynamics simulations. Schematics of the systems with (a) OA and (b) 4C hydrocarbon ligands. Simulated carbon atom density on the surface of (c) OA-5CT and (d) 4C-5CT QDs. The COM distance between 5CT and rubrene started from (e) 1 nm and (d) 2.7 nm initial distances.

measurements (Figure S7 and Table S2). Conversely, when 5CT mediator ligands were attached to the QDs, both OA-5CT and 4C-5CT exhibited substantial decay in the photobleaching features within the measurement time window (Figure 3b,e; see Figure S21a for 8C-5CT). This decay is attributed to triplet energy transfer from the QDs to the 5CT mediator ligands, corresponding to the TET1 process.[21,22,38,54] We also observed that the formation of triplet in 5CT is consistent with the decay of photobleaching in the QDs. Notably, the decay kinetics of both samples were highly similar (Figure 3h; Table S9 showing fitting results). We calculated the rate constants for TET1 (k_{TET1}) for both OA-5CT and 4C-5CT, finding both of them to be approximately 2.0 ns^{-1} (see Table S8 and Supporting Information for calculation). Thus, we conclude that the change of hydrocarbon ligand shell has a negligible effect on TET1. This is reasonable, as 5CT ligands are directly bound to the surface of the QDs, and the distance between them is primarily determined by the length and structure of the mediator's functional group.[38] Reducing the length of the hydrocarbon ligands, which are bound to other sites on the QD, is unlikely to influence the distance between the mediator and the QD. Therefore, the impact on TET1 is expected to be negligible. The fs-TA measurements were also carried out on 8C-5CT, and the results are also consistent with those of OA-5CT and 4C-5CT (Figure S21c).

Additionally, the subsequent introduction of the rubrene annihilator molecules into the OA-5CT, 8C-5CT, or 4C-5CT systems did not induce noticeable changes in the TA features of the QDs in the NIR range (Figure 3c and f, Figure S21b). The decay kinetics of excitons in QDs are almost identical to those in the absence of rubrene annihilators (Figure 3h, Figure S21c). This confirms that the direct TET from QDs to rubrene remains relatively minor, and the modifications of the hydrocarbon ligand shell are unlikely to cause noticeable changes to the decay kinetics of the TA features. We also observed no obvious differences in the exciton decay kinetics when the QDs were directly mixed with rubrene in the absence of 5CT (Figures S16–S18). These findings are consistent with the previously discussed upconversion QY results. With these, we confirm that shorter hydrocarbon ligands have minimal impact on both TET1 and direct TET from QDs to rubrene (Figure 3i).

We therefore hypothesized that the observed improvements in upconversion efficiency stem from enhanced transfer processes outside the QD core, i.e., TET2 from 5CT mediators to rubrene annihilators. To verify this hypothesis, we further investigated the triplet exciton kinetics in the 5CT mediator ligands by examining the TA features in the visible range. As triplet excitons in organic molecules normally have longer lifetimes (in the microsecond range),[56] we conducted nanosecond (ns-) TA measurements on the samples. Broad photoinduced absorption (PIA, negative $\Delta T/T$) features can be observed within the 400–700 nm range for both OA-5CT and 4C-5CT (Figure 4a,b). These features, with lifetimes in the microsecond (μs) range, are consistent with the triplet excitons in 5CT, as previously reported by multiple groups.[11,38,53] The generation of the PIA features aligns with the decay of the excitons within the QDs (see Figure S19, Figure S20, and Notes), further confirming that the PIA features correspond to triplet population in 5CT mediator ligands. The average lifetimes of the 5CT triplet excitons in both OA-5CT and 4C-5CT are approximately 2.3 μs (Figure 4c and Table S11), indicating that the change in the ligand shell is unlikely to affect the 5CT triplet exciton lifetimes prior to the incorporation of rubrene annihilator (also see Figure S21e for 8C-5CT).

To elucidate the kinetics of TET2 from 5CT to rubrene, we conducted further TA measurements by incorporating rubrene into OA-5CT, 8C-4CT, and 4C-5CT solutions. The concentration of QDs was kept at 0.5 mg mL^{-1} in order to

https://doi.org/10.1021/acsnano.5c22144
ACS Nano XXXX, XXX, XXX−XXX

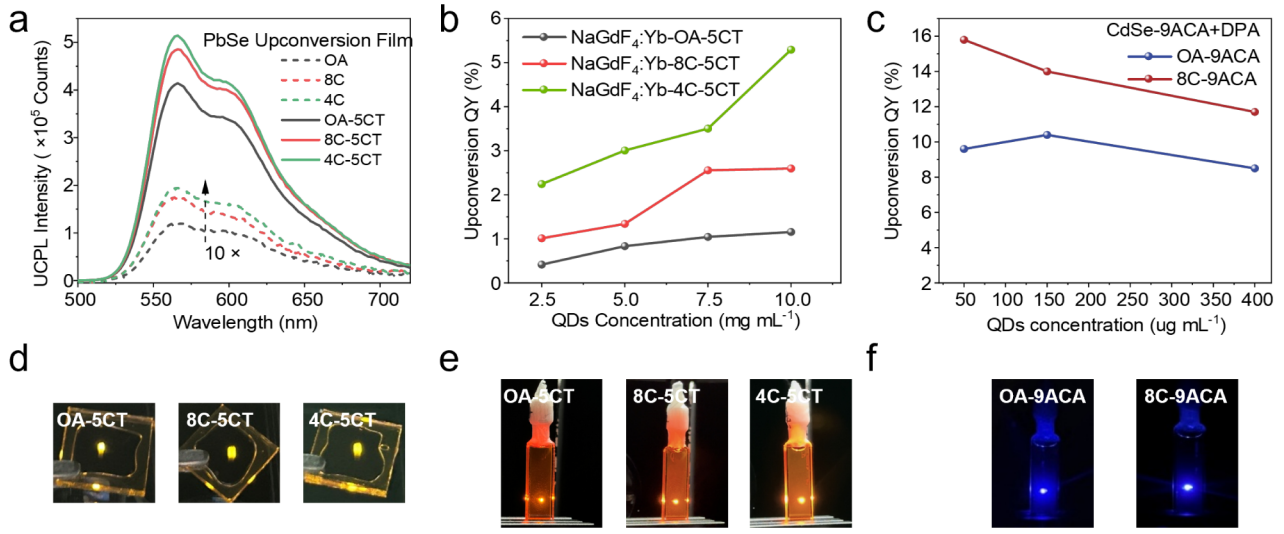

Figure 6. (a) Relative upconversion PL spectra of film samples with QDs possessing different ligand proximities; those without 5CT mediators are scaled up by 10. (b) Upconversion QYs of $NaGdF_4$:Yb nanoparticle-sensitized systems (at different concentrations). Shorter hydrocarbon ligands clearly lead to higher QYs. (c) Upconversion QYs of CdSe QD-based systems (at different concentrations); shorter hydrocarbon ligands also lead to higher QYs. Photographs of the (d) PbSe QD-sensitized upconversion solid-state thin films, (e) solution-phase $NaGdF_4$:Yb nanoparticle-sensitized upconversion systems, and (f) CdSe QD-based upconversion systems (green-to-blue).

maintain adequate overall probe beam transmission, while rubrene at various concentrations was added. We observed transitions of TA features from the triplet states of 5CT to those of rubrene in all samples, confirming the occurrence of TET2 processes (Figure S22).[38] The decay kinetics of the triplet excitons in 5CT are summarized in Figure 4d,e (also see Figure S21, Figure S22, and Note for details). The decay of triplet excitons in 5CT for all samples accelerated with increasing rubrene concentration. Closer inspection of Figure 4d,e shows that the 5CT triplet decay accelerates more steeply with the rubrene concentration for 4C-5CT than for OA-5CT. This difference reflects the interplay between triplet diffusion through the rubrene matrix and the final triplet transfer. At the same rubrene concentration, the mediator in 4C-5CT sits closer to the effective surface of the ligand shell, where the rubrene molecules can easily access. In OA-5CT, the mediator is further away from the shell surface, so the triplet in 5CT has to diffuse further before it can meet an annihilator. As TET2 is simply diffusion followed by the short Dexter transfer, the extra diffusion length in OA-5CT slows the overall process and weakens the concentration dependence, whereas the compact shell in 4C-5CT allows the same encounter-limited regime to be reached at lower concentration, giving the steeper acceleration (Figure 4f, Figure S21f and Figure S23). At the highest possible rubrene concentration of 20 mM, we estimated the TET2 decay rate constant (k_{TET2}) to be 1.62 μs^{-1} for OA-5CT, and it is enhanced to 4.33 μs^{-1} for 4C-5CT (see Table S10 and Supporting Information for calculations). This confirms that the TET2 process is significantly faster in 4C-5CT. The triplet exciton transfer efficiency is also improved from 59.4% for OA-5CT to 93.5% for 4C-5CT at 20 mM rubrene (a 1.57-fold increase, Table S10). Given that the TET1 efficiencies for OA-5CT and 4C-5CT are similar, and assuming the TTA efficiency of rubrene is also comparable in both samples, the increased TET2 efficiency should be reflected in the upconversion QYs. According to Table S6, under conditions of 0.5 mg mL^{-1} QDs and 20 mM rubrene, the upconversion QYs are 0.91% for OA-5CT and 1.37% for 4C-5CT (a ~1.50-fold increase), respectively. The enhancements in the TET2 efficiency are consistent with the observed improvements in upconversion QYs. Therefore, we conclude that the change of ligand proximity can indeed improve the overall upconversion performance via enhanced TET2 processes, where a shorter distance between the 5CT mediator ligand and the rubrene annihilator can be achieved (Figure 4g).

To gain deeper insights into how the hydrocarbon ligands influence the TET2 mechanisms, we further carried out molecular dynamics simulations of rubrene interactions with 5CT mediator ligands anchored on the surface of QDs (see Experimental Methods Section for detailed methods). Since lead chalcogenide QDs typically exhibit an octahedral shape when their size is smaller than 3 nm, we focused on the dominating exposed (111) facets composed of Pb atoms.[59] We attached 5CT mediator ligands with either OA (Figure 5a) or 4C (Figure 5b) ligands to the QD surface, and the system was exposed to toluene solvent (Figure S24). The conformation of the ligands on the QD surface can be characterized by the density distribution of carbon atoms (Figure 5c,d). The simulations revealed that OA-5CT ligands extend approximately 2 nm above the QD surface, whereas 4C-5CT ligands terminate at 1 nm. The average carbon count is also generally higher for OA-5CT. These results align with our expectations, as OA (with 18 carbons) has a longer hydrocarbon chain than 4C.

To investigate the interaction with the acceptor, we placed the system in solvent and simulated the time-dependent center of mass (COM) distance between 5CT and rubrene, starting from two positions: near (1 nm) and far (2.7 nm). Regardless of the initial position, the 4C-5CT system consistently exhibited a stable adsorption state (maintained at ~0.7 nm for ~15 ns, Figure 5e,f), resulting in a short average distance of 1.9 nm over the 50 ns simulation. In contrast, the OA-5CT system showed random diffusion with no obvious adsorption, yielding larger average distances (2.1−2.9 nm). We attribute the adsorption in 4C-5CT to the reduced steric hindrance of the short ligands, which allows rubrene to penetrate the ligand

https://doi.org/10.1021/acsnano.5c22144
ACS Nano XXXX, XXX, XXX−XXX

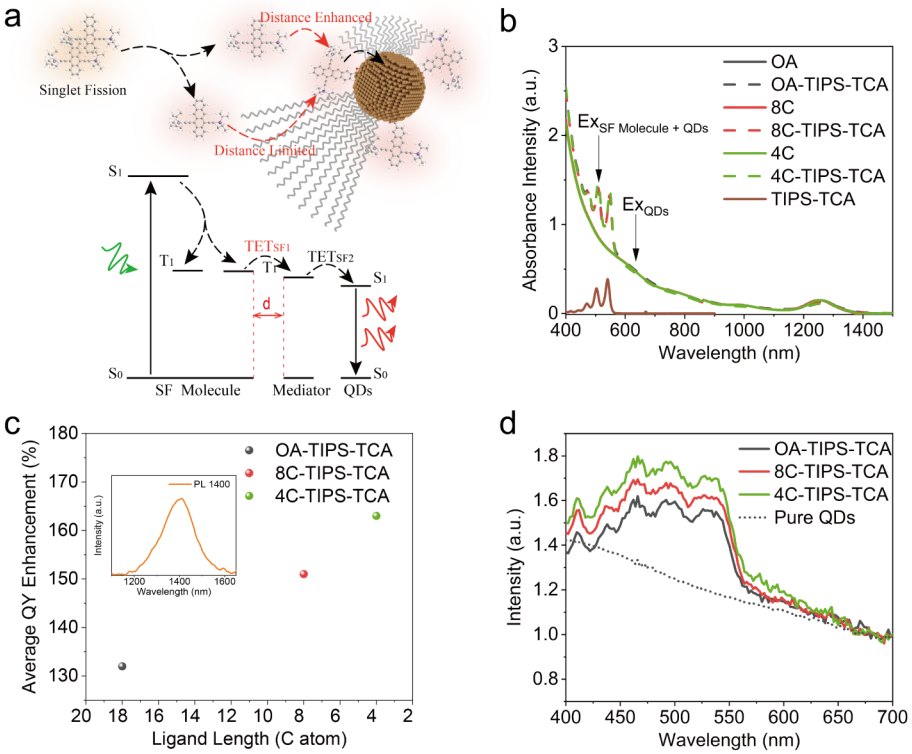

Figure 7. Molecular singlet fission (SF)-based downconversion (SF-DC) using QDs as NIR photon emitter. (a) Schematics of SF in TIPS-Tc molecules and the subsequent TET to TIPS-TCA and QDs, followed by photon re-emission. (b) Absorption spectra of the QDs before and after attachment of TIPS-TCA ligands. (c) QY enhancement calculated by comparing QY under 510 and 635 nm excitation sources. The inset shows the emission spectra of QDs. (d) QD PL excitation spectra of SF-DC solutions with different ligands. The excitation spectra are normalized to the intensity at 700 nm.

shell and engage in stable van der Waals contact with 5CT (Figure S25c-d). These results support our hypothesis that shorter hydrocarbon ligands enable a smaller average distance between the mediator and the annihilator. Two factors may contribute to the reduced steric hindrance in 4C-5CT: (1) the shorter hydrocarbon ligand chain allows for a reduced contact distance between rubrene and 5CT; and (2) the 4C ligands are likely too short to interact with the adsorbed rubrene, whereas the long-chain OA ligands may "sweep" rubrene away through rocking or vibration (also see Supporting Information Videos). Nevertheless, we emphasize that the adsorption of rubrene onto 5CT is likely important, as a relatively static and short rubrene-5CT distance would afford a higher probability of TET compared with random, transient contact events. This observation may also explain why the triplet decay of 5CT accelerates more sharply with increasing rubrene concentration in the 4C-5CT system than in the OA-5CT system, as discussed earlier (Figure 4d,e).

Our strategy to enhance TET2 and thereby improve upconversion performance by optimizing ligand shell compactness is expected to be broadly applicable across various material systems and configurations. Here, we demonstrate that this strategy is also effective in three systems, including: (1) solid-state upconversion thin films based on the same PbSe QD system; (2) a lanthanide nanoparticle-based upconversion system; and (3) a green-to-blue upconversion system based on cadmium selenide (CdSe) QDs as the sensitizers.

The upconversion thin films were fabricated via spin-coating the mixtures of PbSe QD sensitizers mentioned above (with varying ligand proximities) and rubrene. Upon excitation with an 808 nm NIR laser, clear upconversion PL signals were observed, and we found that the upconversion PL intensities increase with shorter hydrocarbon ligands (Figure 6a). Films incorporating 5CT-bonded QDs exhibited more pronounced upconversion PL, visible to the naked eye (Figure 6d), with intensity also increasing as the hydrocarbon ligand length decreased. The measured QYs of the thin films also follow the same trend (Figure S26 and Note for details), implying that the compact ligand strategy is also effective in upconversion solid-state films. We further confirmed that the thermostability of the upconversion films is not affected by the shorter hydrocarbon ligands (Figure S28), indicating that the strategy is suitable for practical applications.

We also extended our study of NIR-to-visible upconversion by employing lanthanide-doped nanoparticles as the sensitizer. Recently, it has been demonstrated that ytterbium-doped sodium gadolinium fluoride ($NaGdF_4$:Yb) nanoparticles can serve as efficient triplet sensitizers for organic molecules.[60,61] As the energy corresponding to the lowest excited state ($^2F_{5/2}$) of Yb^{3+} is 1.26 eV (~980 nm), which is above the triplet energy of both 5CT and rubrene, $NaGdF_4$:Yb nanoparticles should be eligible as the triplet sensitizer in the same TTA system. We therefore constructed $NaGdF_4$:Yb-sensitized upconversion hybrid materials in a similar way, i.e., exchanging the native oleate ligands to short-chain hydrocarbon ligands, followed by the attachment of the 5CT mediator and mixing them with concentrated rubrene annihilators. A 980 nm NIR laser was used as the excitation source. All samples based on the $NaGdF_4$:Yb sensitizers showed bright upconversion PL, and the intensity improves with shorter hydrocarbon ligands, where the difference is visible to the naked eye (Figure 6e). As summarized in Figure 6b, at a series of $NaGdF_4$:Yb

https://doi.org/10.1021/acsnano.5c22144
ACS Nano XXXX, XXX, XXX−XXX

concentrations, the upconversion QYs are consistently the highest for nanoparticles with 4C-5CT ligands, followed by 8C-5CT and OA-5CT. The highest QY (at 10 mg mL^{-1} sensitizer concentration) improved from 1.2% for those with OA-5CT, to 2.6% and 5.3% with 8C-5CT and 4C-5CT ligands, respectively. This trend is exactly the same as that in the QD-sensitized systems. Therefore, we conclude that our ligand proximity strategy is also applicable in lanthanide-doped nanoparticle-sensitized upconversion systems.

To demonstrate that our strategy is also applicable for materials in different wavelength ranges, we extended the work to a well-studied green-to-blue upconversion hybrid materials system, which consists of cadmium selenide (CdSe) QDs, 9-anthracene carboxylic acid (9ACA) mediator ligands, and 9,10-diphenylanthracene (DPA) annihilators.[20−22,27,62−65] The upconversion QYs for these materials are summarized in Figure 6c. Utilizing the original OA hydrocarbon ligands in conjunction with 9ACA ligands, we obtained the highest upconversion QY of approximately 10.4%. When shorter hydrocarbon ligands were employed, the highest QY was notably enhanced to 15.8%, a result that was consistent with the visually brighter upconversion emission observed (Figure 6f). This outcome confirms that our compact ligand strategy is applicable not only in NIR-to-visible upconversion but also in green-to-blue systems and likely more wavelength ranges.

To further examine the versatility of our strategy, we extended our study on an SF-DC hybrid system, where bis((triisopropylsilyl)ethynyl) tetracene (TIPS-Tc) molecules serve as the exciton multiplier via singlet fission, 6,11-bis((triisopropylsilyl)ethynyl)tetracene-2-carboxylic acid)) (TIPS-TCA) ligands serve as triplet mediators, and PbSe QDs serve as the final triplet acceptor and photon re-emitter (Figure 7a). We note that such material combinations have been proven feasible in converting a visible photon into multiple NIR photons,[7−10] and the process is essentially opposite to the upconversion system discussed above. Here, we hypothesize that the ligand strategy can also improve the TET outside the QD core, i.e., the TET from TIPS-Tc singlet fission molecules to the TIPS-TCA mediators (Figure 7a). We synthesized PbSe QDs with a band gap of ∼1 eV (corresponding to the first exciton peak at 1240 nm), slightly below the triplet energy of the TIPS-TCA mediator (approximately 1.1−1.2 eV).[8] Ligand exchange processes were carried out on the QDs, followed by the attachment of the TIPS-TCA mediators. Similar to those in the upconversion systems, we observed no noticeable changes in the absorption features of the QDs after exchanging OA with 8C or 4C, and the additional absorption features from TIPS-TCA indicate successful attachment of the mediators (the samples are referred to as OA-TIPS-TCA, 8C-TIPS-TCA, and 4C-TIPS-TCA, respectively).

The QDs were then added into a concentrated TIPS-Tc solution (∼200 mg mL^{-1}), which generates multiple triplets from each photon via SF. The performance of photon multiplication can be assessed by comparing the NIR QY when selectively exciting either the QDs or the SF molecules in the hybrids, as photon multiplication only occurs when TIPS-Tc SF molecules are excited, and they only absorb photons below 550 nm (Figure 7b).[8,66] We therefore excited the hybrids with either a 635 or a 510 nm laser. From time-resolved PL measurements, we found that the NIR PL lifetimes from QDs for all samples were substantially increased from ∼0.9 μs to over 6 μs when excited by 635 and 510 nm lasers, respectively (Figure S32). Such significantly prolonged lifetimes confirm that when the TIPS-Tc molecules are excited, the SF-generated long-lived triplet excitons are involved in QD NIR emission through TET. The QY enhancement (i.e., the ratio of photon multiplication) can be calculated by comparing their corresponding QY under the two excitation sources,[7,10] i.e., QY_{510}/QY_{635}, as shown in Figure 7c (also see Table S13). Three samples for each hydrocarbon ligand were prepared and tested, and we found that the average QY enhancement is consistently the highest for 4C-TIPS-TCA, followed by 8C-TIPS-TCA and OA-TIPS-TCA (Figure 7c). The average QY enhancement for OA-TIPS-TCA was 132%, and it improved to 151% for 8C-TIPS-TCA and 163% for 4C-TIPS-TCA. This trend is consistent with all the upconversion systems reported in this work. PL excitation (PLE) spectra of the samples were also collected by monitoring the QD NIR PL intensity with different excitation wavelengths (Figure 7d). Compared to that of pure QDs, the PLE spectra for downconversion samples exhibit extra features within the range of 425−550 nm, which correspond to the absorption of TIPS-Tc SF molecules.[7,8] The contribution of TIPS-Tc in the PLE spectra consistently increased from OA-TIPS-TCA to 8C-TIPS-TCA and 4C-TIPS-TCA, which indicates more efficient TET when the hydrocarbon ligands are shorter. With these results, we confirm that our strategy is also effective in SF-DC systems.

Given the above results, we suggest that our strategy holds broad potential for enhancing energy transfer efficiency in a wide range of material systems that rely on the interfaces between nanomaterials and small molecules. This includes not only other QD-based upconversion systems,[11,25,53] but also extends to downconversion materials,[8,9] lanthanide-based hybrid materials,[61] possible metal cluster hybrid materials,[67−69] and more.

CONCLUSIONS

In summary, a general strategy that can overcome the current limitations of TET in various QD-organic hybrid materials has been demonstrated. For TTA-UC, we have shown that shorter hydrocarbon ligands on QDs can remotely enhance TET2, hence improving the overall TET and upconversion efficiency in hybrid materials comprising PbSe QDs, 5CT mediator ligands, and rubrene triplet annihilators. This enhancement is attributed to the altered surface ligand shell compactness on the QDs, which facilitates closer contact between the mediators and annihilators, thereby accelerating triplet transfer beyond the QD core. Through comprehensive photophysical characterizations, we have confirmed that our strategy primarily improves the rate and efficiency of TET2 from the mediator ligand to the annihilator, while maintaining efficient TET1, thereby supporting our hypothesis. Further simulation results suggest that stronger adsorption of rubrene onto 5CT occurs in 4C-5CT, due to reduced steric hindrance from the shorter, proximal hydrocarbon ligands. This ligand proximity strategy is effective not only in solution-based systems but also in solid-state upconversion thin films fabricated from the same materials. Additionally, we have successfully applied this strategy to other upconversion material systems, including CdSe QD- and lanthanide-doped nanoparticle-sensitized systems. The same principle also applies in molecular SF-DC hybrids employing QDs as photon emitters, where a significant improvement in the photon-multiplication efficiency was achieved by the same strategy. We suggest that the ligand shell on nanoparticles affects not only energy transfer where

https://doi.org/10.1021/acsnano.5c22144
ACS Nano XXXX, XXX, XXX−XXX

the core is involved but also beyond the core. The compact ligand proximity strategy proposed in this work is broadly applicable across a wide range of material systems and applications that rely on energy transfer at the interfaces between nanomaterials and semiconductor organic molecules.

EXPERIMENTAL METHODS

Materials

Oleic acid (OA, tech grade, 90%), 1-octadecene (ODE, 90%), selenium powder (Se, 99.999%), cadmium oxide (CdO, 99.99%), octanoic acid (8C, 99%), and butyric acid (4C, 99%) were purchased from Sigma-Aldrich. Bis((triisopropylsilyl)ethynyl) tetracene (TIPS-Tc) and 6,11-bis((triisopropylsilyl)ethynyl)tetracene-2-carboxylic acid)) (TIPS-TCA) were purchased from Zhengzhou Alfa Chemical Co., Ltd. Lead oxide (PbO, 99.999%) was purchased from Aladdin. Tri-n-octylphosphine (TOP, 70%) was purchased from Macklin. HPLC-grade *n*-hexane, toluene, tetrahydrofuran, and acetone were purchased from Chron Chemicals.

QDs Synthesis

The synthesis of PbSe was performed by modifying previously published work.[70] PbO (0.45 g), OA (1.62 mL), and ODE (12.67 mL) were mixed in a 50 mL three-neck flask and degassed under vacuum at 80 °C, and the mixture was further heated to 110 °C under vacuum for 1.5 h. Pb oleate was formed, as indicated by the discoloration of the reaction to a clear solution. Then the reaction atmosphere was switched to N_2, and the reaction temperature was set to 120 °C. 7.5 mL of selenium-trioctylphosphine solution (containing 0.64 g of selenium, 1.00 mmol) was then quickly injected into this hot solution. Immediately after injection, the heater was turned off, and the solution was transferred to a water bath for controlled cooling. When the temperature dropped to 60 °C, the reaction solution was cooled by injection of 5 mL of hexane. The PbSe QDs were washed 3 times by adding a 1:3 hexanes/acetone mixture, followed by centrifuging at 7500 rpm for 3 min. The supernatant was discarded. The final pellet was stored in the dark inside the glovebox for future use.

The synthesis of CdSe was performed by modifying previously published work.[71] CdO (0.512 g), OA (3.5 mL), and ODE (32 mL) were mixed in a 50 mL three-neck flask and degassed under vacuum at 80 °C. The mixture was further heated to 110 °C under vacuum for 1.5 h. Subsequently, the temperature was raised to 260 °C. After the solution became clear, it was maintained at 260 °C for 5−10 min. The temperature was then lowered to 120 °C, and the system was purged with nitrogen three times. Following this, the temperature was increased to 245 °C, at which point a suspension of 0.316 g of selenium powder dissolved in 5 mL of ODE was swiftly injected. The reaction mixture was allowed to cool to 175 °C, followed by cooling to room temperature using a water bath. The resulting CdSe QDs were purified by precipitation with anhydrous ethanol/hexane and isolated via centrifugation, with this purification cycle repeated three times.

5CT Synthesis

5CT was synthesized following previously published work.[72,73]

$NaGdF_4$:Yb Synthesis

The lanthanide nanocrystals were synthesized via a coprecipitation method.[74] For $NaGdF_4$:Yb (50 mol %) nanocrystals: $Gd(CH_3CO_2)_3$ (0.2 mmol) and $Yb(CH_3CO_2)_3$ (0.2 mmol) were mixed with OA (6 mL) and octadecene (9 mL) in a 50 mL flask and heated at 150 °C for 2 h. The mixture was cooled to 50 °C, and a methanol solution (6 mL) containing NaOH (2.5 mmol) and NH_4F (4 mmol) was added, followed by stirring for 12 h. The temperature was raised to 100 °C to evaporate methanol, and then the reaction proceeded at 270 °C for 1 h under nitrogen. After cooling to room temperature, the nanocrystals were precipitated with ethanol/hexane, collected by centrifugation at 12,000 rpm for 5 min, and redispersed in hexane.

Ligand Exchange of PbSe/CdSe QDs with 8C or 4C

The ligand exchange of PbSe QDs was performed by modifying previously published work.[67] In brief, the purified QDs (50 mg mL^{-1} in toluene) were first loaded into separate sample vials in a nitrogen-filled glovebox. The liquid-phase ligands (8C and 4C) were slowly added to the QD dispersion by using a micropipette. ∼0.08 mmol of ligands was added to 12.5 mg of QDs. After the ligands were added, the QD dispersions were stirred for about 40 min. The exchanged QDs were purified by adding extra toluene and acetonitrile, followed by centrifugation. The purification process was repeated twice more to remove the residual ligands. The purified QDs were then dispersed in toluene at a concentration of ∼20 mg mL^{-1} and filtered. The hexane solvent was then removed by vacuum drying. The QDs were finally dispersed at concentrations of 20 mg mL^{-1} and 10 mg mL^{-1} for upconversion and 5CT ligand exchange.

The ligand exchange of CdSe QDs was performed as follows. Purified QDs (50 mg ml^{-1} in toluene) were first loaded into separate sample vials in a nitrogen-filled glovebox. The liquid phase ligands 8C were slowly added to the QDs dispersion using a micropipette. ∼0.08 mmol of ligands was added to 10 mg of QDs. After the addition, the QD dispersions were further stirred for about 40 min. The exchanged QDs were purified by adding extra toluene and acetonitrile, followed by centrifugation.

Ligand Exchange of PbSe/CdSe QDs with 5CT/9ACA Mediators

PbSe ligand exchange was performed according to the literature with some modifications.[56] In brief, 5 mg of PbSe QDs capped with OA/8C/4C ligands and 2 mg of 5CT were mixed in 0.4 mL of toluene and stirred for 40 min. Then, 0.4 mL of this ligand exchange solution was precipitated by adding 1.2 mL of acetone, followed by centrifugation at 8000 rpm for 5 min. The pellet at the bottom was redispersed in 0.4 mL of toluene solution. The 5CT-functionalized QDs with different ligands were labeled OA-5CT, 8C-5CT, and 4C-5CT.

CdSe ligand exchange was performed according to the literature with some modifications.[62] In brief, 5 mg of CdSe QDs capped with OA/8C ligand and 15 mg of 9ACA were mixed in 0.4 mL of THF and stirred for 2 h. Then, 0.4 mL of this ligand exchange solution was precipitated by adding 1.2 mL of acetone, followed by centrifugation for 5 min at 8000 rpm. The pellet at the bottom was redispersed in 0.4 mL of toluene solution. The 9ACA-functionalized QDs with different ligands were labeled OA-9ACA and 8C-9ACA.

Ligand Exchange of PbSe QDs with TIPS-TCA

PbSe ligand exchange was performed according to the literature with some modifications.[8] 5 mg of PbSe/QDs capped with OA/8C/4C ligand and 5 mg of TIPS-TCA were mixed in a toluene/THF mixture of 5:1 and stirred for 40 min. Then, 0.25 mL of this ligand exchange solution was precipitated by adding 1 mL of acetone, followed by 5 min of centrifugation at 8000 rpm. The pellet at the bottom was redispersed in 0.125 mL of toluene solution with 200 mg mL^{-1} TIPS-Tc. The TIPS-TCA-functionalized QDs with different ligands were labeled OA- TIPS-TCA, 8C- TIPS-TCA, and 4C- TIPS-TCA.

Estimation of the Number of 5CT/9ACA Mediator Ligands per PbSe/CdSe QDs

PbSe QDs capped with 5CT were dispersed in toluene. Figure 1e shows the absorption spectrum in toluene. Since the absorption spectra of 5CT and PbSe QDs overlap in the visible range, in order to calculate the number of bound ligands, the contribution of the QDs must be taken into account. The differential spectrum (Figure 1f) was obtained by subtracting the QD contribution from the 5CT/PbSe spectrum (Figure 1e), which was used to estimate the number of bound 5CT ligands. Note that the redshift in the bound 5CT absorption (Figure 1f) confirms successful ligand exchange. The extinction coefficient of 5CT at 482 nm is 5.3×10^3 $M^{-1}cm^{-1}$.[24,38] The diameter of the PbSe QDs is ∼2.7 nm (Figure S2). Using these values and Lambert−Beer law, we calculated the average number of 5CT ligands per PbSe QD to be ∼12.

https://doi.org/10.1021/acsnano.5c22144
ACS Nano XXXX, XXX, XXX−XXX

CdSe QDs capped with 9ACA were dispersed in toluene. Figure S31 shows the absorption spectrum in toluene. Since the absorption spectra of 9ACA and CdSe QDs overlap in the visible region, in order to calculate the number of bound ligands, the contribution of the QDs must be taken into account. The differential spectrum (Figure S31b) was obtained by subtracting the QD contribution from the 9ACA/CdSe spectrum (Figure S31a), which was used to estimate the number of bound 9ACA ligands. The extinction coefficient of 9ACA at 389 nm is 7.8×10^3 $M^{-1}cm^{-1}$.[22] The diameter of the CdSe QDs is ~2.5 nm (Figure S29b). Using these values and Lambert–Beer law, we calculated the average number of 5CT ligands per CdSe QD to be ~14.

Preparation of Samples for Transient Absorption and Upconversion Measurements

For upconversion samples, PbSe QDs were dispersed in 20 mM rubrene solution at concentrations of 0.25, 0.5, 1, and 2 mg mL^{-1}, respectively, followed by transfer into cuvettes with a 1 mm optical path length. CdSe QDs were dispersed in 7 mM rubrene solution at concentrations of 50, 150, and 400 μg mL^{-1}, respectively, followed by transfer into cuvettes with a 1 mm optical path length. CdSe QDs were dispersed in 7 mM rubrene solution at concentrations of 50, 150, and 400 μg mL^{-1}, respectively, followed by transfer into cuvettes with a 1 mm optical path length. $NaGdF_4$:Yb nanocrystals were dispersed in 20 mM rubrene solution at concentrations of 2.5, 5, 7.5, and 10 mg mL^{-1}, respectively, followed by transfer into cuvettes with a 1 mm optical path length. For upconversion thin film samples, PbSe QDs were dispersed in 20 mM rubrene solution at a concentration of 1 mg mL^{-1}. Then, a thin film was formed by rotating the soda-lime glass substrate at 3000 rpm for 30 s. For transient absorption measurements probing at 840–1300 nm, samples with optimal upconversion QY were redispersed in toluene and transferred to a 2 mm path length cuvette. For probe measurements in the 400–700 nm without rubrene, the PbSe concentration was maintained at 2 mg mL^{-1}. When rubrene was incorporated, the PbSe concentration was reduced to 0.5 mg mL^{-1}. All samples were prepared in a nitrogen-filled glovebox.

Preparation of Samples for Singlet Fission Measurements

For singlet fission samples, PbSe-TIPS-TCA QDs were dispersed in a concentrated TIPS-tetracene solution (200 mg mL^{-1}) at a concentration of 40 mg mL^{-1} and then transferred to a 0.2 mm borosilicate capillary tube. The PLQYs of the samples were measured by using 510 and 635 nm lasers.

Upconversion Quantum Yield (QY) Measurement

The upconversion QY is calculated by comparison to a rubrene reference excited at 520 nm. The photon upconversion QY, Φ_{UC} is calculated as

$$\Phi_{UC} = 2 \times \Phi_{reference} \times \frac{\text{photons absorbed by reference}}{\text{photons absorbed by UC sample}} \times \frac{PL_{UCsample}}{PL_{reference}} \quad (1)$$

$$\text{photons absorbed} = \frac{\text{laser power}}{hc/\lambda} \times (1 - 10^{-Abs}) \quad (2)$$

where $\Phi_{reference}$ is the photoluminescence QY of the rubrene reference, which is 79% in toluene (measured by an Edinburgh FLS1000 spectrometer with an integrating sphere).

Transient Absorption Spectroscopy

Transient absorption spectra were collected using an integrated Helios and EOS setup (Ultrafast Systems LLC) operating in a nondegenerate pump–probe configuration. Femtosecond transient absorption spectra (TAS) were recorded on an integrated Helios spectrometer (Ultrafast Systems LLC) configured in a nondegenerate pump–probe geometry. The light source was a one-box Ti:sapphire regenerative amplifier (Coherent Astrella F, 800 nm center wavelength, 1 kHz repetition rate, and 100 fs pulse duration). The output was split into two arms. One arm was directed through separate β-barium borate (BBO) crystals to produce a 780 nm pump. Another arm was transformed into a white-light continuum probe pulse (420–1700 nm) via sapphire and YAG crystals. In the nanosecond TAS setup, the pump is the same as in the femtosecond TAS setup, and the probe is generated by a 20 kHz WLC laser, whose pulse duration is less than 1 ns. The delay is controlled electronically. A 750 nm long-pass filter was placed before the sample to ensure spectral purity.

Steady-State Absorption and Photoluminescence Spectroscopy

Absorption spectra were measured using a Lambda 1050+. Photoluminescence spectra were measured by an Edinburgh FLS1000. The upconversion spectra were measured by an Edinburgh FLS1000 with another 808 nm continuous-wave laser.

HR-TEM

Transmission electron microscopy samples were prepared by depositing 2–3 drops of PbSe quantum dots dissolved in a hexane solution onto ultrathin carbon support films in a nitrogen-filled glovebox using a JEM 2100F.

Small-Angle X-ray (SAXS) Scattering

The small-angle X-ray scattering data were collected on a Xenocs Xeuss 3.0 instrument equipped with a D2+ MetalJet X-ray source (Excillum, Ga Kα, λ = 0.154 nm). The beam size was less than 0.5 × 0.5 mm^2. Scattered X-rays were captured on a 2-dimensional Pilatus detector. The scattering vector (q) was calibrated using a standard silver behenate with the primary reflection peak at 1.076 nm^{-1}.

Nuclear Magnetic Resonance Spectroscopy (NMR)

All NMR spectra were recorded on JEOL NMR instruments at 500 MHz for ^{1}H NMR. All spectra were recorded at 25 °C. Chemical shifts are reported in parts per million (ppm, δ), downfield from tetramethylsilane (TMS, δ=0.00 ppm) and are referenced to residual solvent (^{1}H NMR: δ = 7.26 ppm for $CDCl_3$). The $Fe(C_5H_5)_2$ (^{1}H NMR: δ = 4.16 ppm) was used as an internal standard to determine the ratio of ligand.

X-ray Diffraction (XRD)

XRD measurements were performed using a MiniFlex600 with Cu Kα radiation (λ = 1.5406 Å). Diffractograms were collected within an angular range of 10–80°.

Thermogravimetric Analysis (TGA)

TGA measurements were performed using a Mettler Toledo/TGA2 at a heating rate of 10 K min^{-1}.

Fourier Transform Infrared (FTIR) Spectroscopy

FTIR measurements were performed using a JASCO FT/IR-4X spectrometer.

Molecular Dynamics (MD) Simulations

All MD simulations were performed using the GROMACS 2024.2 package.[75] The organic components (5CT, OA, 4C, Rubrene, and Toluene) were modeled using the Generalized Amber Force Field (GAFF),[76] while the Pb surface was described by the Universal Force Field (UFF).[77] The simulation system was constructed as a periodic box of 3.36 × 3.36 × 8.00 nm, representing a solid–liquid interface. The surface consisted of a single 5CT molecule grafted at the geometric center of the Pb slab, surrounded by 16 randomly grafted ligand molecules (either OA or 4C, to establish distinct systems). The functionalized surface was solvated with one rubrene molecule and approximately 400 toluene molecules.

Prior to the production run, the system underwent energy minimization to remove steric clashes. The production simulation was conducted in the NVT ensemble for 50 ns with a time step of 1 fs. The system temperature was maintained at 298.15 K using the Bussi-Donadio-Parrinello (stochastic velocity rescaling) thermostat.[78] Van der Waals interactions were calculated by using a cutoff radius of 1.2 nm. All bond lengths involving hydrogen atoms were constrained using the LINCS algorithm.[79] The Pb surface atoms were frozen throughout the simulation to mimic the bulk substrate. To ensure statistical reliability, the number density profiles of carbon atoms

https://doi.org/10.1021/acsnano.5c22144
ACS Nano XXXX, XXX, XXX–XXX

along the surface normal (z-axis) were calculated by averaging the trajectory over the final 20 ns.

■ ASSOCIATED CONTENT

Supporting Information

The Supporting Information is available free of charge at https://pubs.acs.org/doi/10.1021/acsnano.5c22144.

XRD, TEM, TGA, NMR, SAXS, time-resolved PL, power-dependent measurements, stability analysis, additional details of TA measurements, molecular simulation, triplet transfer calculation, and discussions (Figures S1−S32; Tables S1−S13, and videos of molecular simulations). (TBC) (PDF)

Video of molecular dynamics simulation for OA-5CT. (MP4)

Video of molecular dynamics simulation for 4C-5CT. (MP4)

■ AUTHOR INFORMATION

Corresponding Authors

Akshay Rao − *Cavendish Laboratory, University of Cambridge, Cambridge CB3 0HE, U.K.;* orcid.org/0000-0003-4261-0766; Email: ar525@cam.ac.uk

Zhilong Zhang − *South China Advanced Institute for Soft Matter Science and Technology, Guangdong Provincial Key Laboratory of Functional and Intelligent Hybrid Materials and Devices, State Key Laboratory of Luminescent Materials and Devices, School of Emergent Soft Matter, South China University of Technology, Guangzhou 510640, China; Cavendish Laboratory, University of Cambridge, Cambridge CB3 0HE, U.K.;* orcid.org/0000-0001-9903-4945; Email: zzhang@scut.edu.cn

Authors

Yanhong Fan − *South China Advanced Institute for Soft Matter Science and Technology, Guangdong Provincial Key Laboratory of Functional and Intelligent Hybrid Materials and Devices, State Key Laboratory of Luminescent Materials and Devices, School of Emergent Soft Matter, South China University of Technology, Guangzhou 510640, China*

Jia Luo − *South China Advanced Institute for Soft Matter Science and Technology, Guangdong Provincial Key Laboratory of Functional and Intelligent Hybrid Materials and Devices, State Key Laboratory of Luminescent Materials and Devices, School of Emergent Soft Matter, South China University of Technology, Guangzhou 510640, China*

Ziqi Wang − *South China Advanced Institute for Soft Matter Science and Technology, Guangdong Provincial Key Laboratory of Functional and Intelligent Hybrid Materials and Devices, State Key Laboratory of Luminescent Materials and Devices, School of Emergent Soft Matter, South China University of Technology, Guangzhou 510640, China*

Yanchao Zhao − *South China Advanced Institute for Soft Matter Science and Technology, Guangdong Provincial Key Laboratory of Functional and Intelligent Hybrid Materials and Devices, State Key Laboratory of Luminescent Materials and Devices, School of Emergent Soft Matter, South China University of Technology, Guangzhou 510640, China*

Shuangke Wu − *South China Advanced Institute for Soft Matter Science and Technology, Guangdong Provincial Key Laboratory of Functional and Intelligent Hybrid Materials and Devices, State Key Laboratory of Luminescent Materials and Devices, School of Emergent Soft Matter, South China University of Technology, Guangzhou 510640, China*

Yuqi Sun − *Cavendish Laboratory, University of Cambridge, Cambridge CB3 0HE, U.K.*

Peng Zhang − *Institute of Biopharmaceutical and Health Engineering, Shenzhen International Graduate School, Tsinghua University, Shenzhen 518055, China;* orcid.org/0009-0000-6634-9350

Haoyu Song − *South China Advanced Institute for Soft Matter Science and Technology, Guangdong Provincial Key Laboratory of Functional and Intelligent Hybrid Materials and Devices, State Key Laboratory of Luminescent Materials and Devices, School of Emergent Soft Matter, South China University of Technology, Guangzhou 510640, China*

Xianggui Zhou − *South China Advanced Institute for Soft Matter Science and Technology, Guangdong Provincial Key Laboratory of Functional and Intelligent Hybrid Materials and Devices, State Key Laboratory of Luminescent Materials and Devices, School of Emergent Soft Matter, South China University of Technology, Guangzhou 510640, China*

Zhiqiang Hu − *Institute of Biopharmaceutical and Health Engineering, Shenzhen International Graduate School, Tsinghua University, Shenzhen 518055, China*

Jiajie Wu − *South China Advanced Institute for Soft Matter Science and Technology, Guangdong Provincial Key Laboratory of Functional and Intelligent Hybrid Materials and Devices, State Key Laboratory of Luminescent Materials and Devices, School of Emergent Soft Matter, South China University of Technology, Guangzhou 510640, China*

Yaqi Gu − *South China Advanced Institute for Soft Matter Science and Technology, Guangdong Provincial Key Laboratory of Functional and Intelligent Hybrid Materials and Devices, State Key Laboratory of Luminescent Materials and Devices, School of Emergent Soft Matter, South China University of Technology, Guangzhou 510640, China*

Lu Qiu − *South China Advanced Institute for Soft Matter Science and Technology, Guangdong Provincial Key Laboratory of Functional and Intelligent Hybrid Materials and Devices, State Key Laboratory of Luminescent Materials and Devices, School of Emergent Soft Matter, South China University of Technology, Guangzhou 510640, China*

Zhuang Miao − *South China Advanced Institute for Soft Matter Science and Technology, Guangdong Provincial Key Laboratory of Functional and Intelligent Hybrid Materials and Devices, State Key Laboratory of Luminescent Materials and Devices, School of Emergent Soft Matter, South China University of Technology, Guangzhou 510640, China*

Sanyang Han − *Institute of Biopharmaceutical and Health Engineering, Shenzhen International Graduate School, Tsinghua University, Shenzhen 518055, China;* orcid.org/0000-0001-7414-7193

Xing Jiang − *South China Advanced Institute for Soft Matter Science and Technology, Guangdong Provincial Key Laboratory of Functional and Intelligent Hybrid Materials and Devices, State Key Laboratory of Luminescent Materials and Devices, School of Emergent Soft Matter, South China University of Technology, Guangzhou 510640, China;* orcid.org/0000-0001-8259-1948

Victor Gray − *Department of Chemistry-Ångström Laboratory, Uppsala University, Uppsala 75120, Sweden;* orcid.org/0000-0001-6583-8654

Jiajia Zhou − *South China Advanced Institute for Soft Matter Science and Technology, Guangdong Provincial Key*

https://doi.org/10.1021/acsnano.5c22144
ACS Nano XXXX, XXX, XXX−XXX

Laboratory of Functional and Intelligent Hybrid Materials and Devices, State Key Laboratory of Luminescent Materials and Devices, School of Emergent Soft Matter, South China University of Technology, Guangzhou 510640, China; orcid.org/0000-0002-2258-6757

Complete contact information is available at: https://pubs.acs.org/10.1021/acsnano.5c22144

Author Contributions

#Y.F., J.L., and Z.W. contributed equally to this work.

Notes

The authors declare no competing financial interest.

■ ACKNOWLEDGMENTS

This work was supported by the National Natural Science Foundation of China (No. 12474031 and W2433157) and the European Union's Horizon 2020 research and innovation programme under the Marie Skłodowska-Curie Actions grant (no. 842271, TRITON project). Z.Z. also acknowledges financial support from Guangdong province (2025A1515010298 and 2023QN10C450s), Guangzhou city (SL2023A04J00824 and 2024A04J3731), and the GJYC program (2024D01J0078 and 2024D03J0007).

■ REFERENCES

(1) Thompson, N. J.; Wilson, M. W. B.; Congreve, D. N.; Brown, P. R.; Scherer, J. M.; Bischof, T. S.; Wu, M.; Geva, N.; Welborn, M.; Voorhis, T. V.; et al. Energy Harvesting of Non-Emissive Triplet Excitons in Tetracene by Emissive PbS Nanocrystals. *Nat. Mater.* **2014**, *13* (11), 1039−1043.

(2) Mongin, C.; Garakyaraghi, S.; Razgoniaeva, N.; Zamkov, M.; Castellano, F. N. Direct Observation of Triplet Energy Transfer from Semiconductor Nanocrystals. *Science* **2016**, *351* (6271), 369−372.

(3) Nienhaus, L.; Wu, M.; Bulović, V.; Baldo, M. A.; Bawendi, M. G. Using Lead Chalcogenide Nanocrystals as Spin Mixers: a Perspective on Near-Infrared-to-Visible Upconversion. *Dalton Trans.* **2018**, *47* (26), 8509−8516.

(4) Huang, Z.; Tang, M. L. Designing Transmitter Ligands That Mediate Energy Transfer between Semiconductor Nanocrystals and Molecules. *J. Am. Chem. Soc.* **2017**, *139* (28), 9412−9418.

(5) Huang, Z.; Lee Tang, M. Semiconductor Nanocrystal Light Absorbers for Photon Upconversion. *J. Phys. Chem. Lett.* **2018**, *9* (21), 6198−6206.

(6) Wu, M.; Congreve, D. N.; Wilson, M. W. B.; Jean, J.; Geva, N.; Welborn, M.; Van Voorhis, T.; Bulović, V.; Bawendi, M. G.; Baldo, M. A. Solid-State Infrared-to-Visible Upconversion Sensitized by Colloidal Nanocrystals. *Nat. Photonics* **2016**, *10* (1), 31−34.

(7) Allardice, J. R.; Thampi, A.; Dowland, S.; Xiao, J.; Gray, V.; Zhang, Z.; Budden, P.; Petty, A. J. I. I.; Davis, N. J. L. K.; Greenham, N. C.; et al. Engineering Molecular Ligand Shells on Quantum Dots for Quantitative Harvesting of Triplet Excitons Generated by Singlet Fission. *J. Am. Chem. Soc.* **2019**, *141* (32), 12907−12915.

(8) Gray, V.; Toolan, D. T. W.; Dowland, S.; Allardice, J. R.; Weir, M. P.; Zhang, Z.; Xiao, J.; Klimash, A.; Winkel, J. F.; Holland, E. K.; et al. Ligand-Directed Self-Assembly of Organic-Semiconductor/Quantum-Dot Blend Films Enables Efficient Triplet Exciton-Photon Conversion. *J. Am. Chem. Soc.* **2024**, *146* (11), 7763−7770.

(9) Gray, V.; Allardice, J. R.; Zhang, Z.; Dowland, S.; Xiao, J.; Petty, A. J. I. I.; Anthony, J. E.; Greenham, N. C.; Rao, A. Direct vs Delayed Triplet Energy Transfer from Organic Semiconductors to Quantum Dots and Implications for Luminescent Harvesting of Triplet Excitons. *ACS Nano* **2020**, *14* (4), 4224−4234.

(10) Gray, V.; Zhang, Z.; Dowland, S.; Allardice, J. R.; Alvertis, A. M.; Xiao, J.; Greenham, N. C.; Anthony, J. E.; Rao, A. Thiol-Anchored TIPS-Tetracene Ligands with Quantitative Triplet Energy Transfer to PbS Quantum Dots and Improved Thermal Stability. *J. Phys. Chem. Lett.* **2020**, *11* (17), 7239−7244.

(11) Liang, W.; Nie, C.; Du, J.; Han, Y.; Zhao, G.; Yang, F.; Liang, G.; Wu, K. Near-Infrared Photon Upconversion and Solar Synthesis Using Lead-Free Nanocrystals. *Nat. Photonics* **2023**, *17* (4), 346−353.

(12) Gholizadeh, E. M.; Prasad, S. K. K.; Teh, Z. L.; Ishwara, T.; Norman, S.; Petty, A. J.; Cole, J. H.; Cheong, S.; Tilley, R. D.; Anthony, J. E.; et al. Photochemical Upconversion of Near-Infrared Light from Below the Silicon Bandgap. *Nat. Photonics* **2020**, *14* (9), 585−590.

(13) Chen, S.; Weitemier, A. Z.; Zeng, X.; He, L.; Wang, X.; Tao, Y.; Huang, A. J. Y.; Hashimotodani, Y.; Kano, M.; Iwasaki, H.; et al. Near-Infrared Deep Brain Stimulation via Upconversion Nanoparticle−Mediated Optogenetics. *Science* **2018**, *359* (6376), 679−684.

(14) Xu, J.; Yang, P.; Sun, M.; Bi, H.; Liu, B.; Yang, D.; Gai, S.; He, F.; Lin, J. Highly Emissive Dye-Sensitized Upconversion Nanostructure for Dual-Photosensitizer Photodynamic Therapy and Bioimaging. *ACS Nano* **2017**, *11* (4), 4133−4144.

(15) Sanders, S. N.; Schloemer, T. H.; Gangishetty, M. K.; Anderson, D.; Seitz, M.; Gallegos, A. O.; Stokes, R. C.; Congreve, D. N. Triplet Fusion Upconversion Nanocapsules for Volumetric 3D Printing. *Nature* **2022**, *604* (7906), 474−478.

(16) Tayebjee, M. J. Y.; McCamey, D. R.; Schmidt, T. W. Beyond Shockley−Queisser: Molecular Approaches to High-Efficiency Photovoltaics. *J. Phys. Chem. Lett.* **2015**, *6* (12), 2367−2378.

(17) Wen, S.; Zhou, J.; Schuck, P. J.; Suh, Y. D.; Schmidt, T. W.; Jin, D. Future and Challenges for Hybrid Upconversion Nanosystems. *Nat. Photonics* **2019**, *13* (12), 828−838.

(18) Schulze, T. F.; Schmidt, T. W. Photochemical Upconversion: Present Status and Prospects for its Application to Solar Energy Conversion. *Energy Environ. Sci.* **2015**, *8* (1), 103−125.

(19) Bharmoria, P.; Bildirir, H.; Moth-Poulsen, K. Triplet−Triplet Annihilation Based Near Infrared to Visible Molecular Photon Upconversion. *Chem. Soc. Rev.* **2020**, *49* (18), 6529−6554.

(20) Olesund, A.; Gray, V.; Mårtensson, J.; Albinsson, B. Diphenylanthracene Dimers for Triplet−Triplet Annihilation Photon Upconversion: Mechanistic Insights for Intramolecular Pathways and the Importance of Molecular Geometry. *J. Am. Chem. Soc.* **2021**, *143* (15), 5745−5754.

(21) De Roo, J.; Huang, Z.; Schuster, N. J.; Hamachi, L. S.; Congreve, D. N.; Xu, Z.; Xia, P.; Fishman, D. A.; Lian, T.; Owen, J. S.; et al. Anthracene Diphosphate Ligands for CdSe Quantum Dots; Molecular Design for Efficient Upconversion. *Chem. Mater.* **2020**, *32* (4), 1461−1466.

(22) Rigsby, E. M.; Miyashita, T.; Jaimes, P.; Fishman, D. A.; Tang, M. L. On the Size-Dependence of CdSe Nanocrystals for Photon Upconversion with Anthracene. *J. Chem. Phys.* **2020**, *153* (11), 114702.

(23) Nienhaus, L.; Wu, M.; Geva, N.; Shepherd, J. J.; Wilson, M. W. B.; Bulović, V.; Van Voorhis, T.; Baldo, M. A.; Bawendi, M. G. Speed Limit for Triplet-Exciton Transfer in Solid-State PbS Nanocrystal-Sensitized Photon Upconversion. *ACS Nano* **2017**, *11* (8), 7848−7857.

(24) Mahboub, M.; Huang, Z.; Tang, M. L. Efficient Infrared-to-Visible Upconversion with Subsolar Irradiance. *Nano Lett.* **2016**, *16* (11), 7169−7175.

(25) Lai, R.; Sang, Y.; Zhao, Y.; Wu, K. Triplet Sensitization and Photon Upconversion Using InP-Based Quantum Dots. *J. Am. Chem. Soc.* **2020**, *142* (47), 19825−19829.

(26) Okumura, K.; Mase, K.; Yanai, N.; Kimizuka, N. Employing Core-Shell Quantum Dots as Triplet Sensitizers for Photon Upconversion. *Chem. - Eur. J.* **2016**, *22* (23), 7721−7726.

(27) Ronchi, A.; Capitani, C.; Pinchetti, V.; Gariano, G.; Zaffalon, M. L.; Meinardi, F.; Brovelli, S.; Monguzzi, A. High Photon Upconversion Efficiency with Hybrid Triplet Sensitizers by Ultrafast Hole-Routing in Electronic-Doped Nanocrystals. *Adv. Mater.* **2020**, *32* (37), 2002953.

(28) Sullivan, C. M.; Bieber, A. S.; Drozdick, H. K.; Moller, G.; Kuszynski, J. E.; VanOrman, Z. A.; Wieghold, S.; Strouse, G. F.;

Nienhaus, L. Surface Doping Boosts Triplet Generation Yield in Perovskite-Sensitized Upconversion. *Adv. Opt. Mater.* **2023**, *11* (1), 2201921.
(29) Würth, C.; Fischer, S.; Grauel, B.; Alivisatos, A. P.; Resch-Genger, U. Quantum Yields, Surface Quenching, and Passivation Efficiency for Ultrasmall Core/Shell Upconverting Nanoparticles. *J. Am. Chem. Soc.* **2018**, *140* (14), 4922−4928.
(30) Chang, K. T.; Liang, W.; Gong, S.; Yeung, P. H.; Feng, J.; Chen, X.; Lu, H. Triplet Sensitization Photon Upconversion Using Near-Infrared Indirect-Bandgap AgBiS2 Nanocrystals. *J. Am. Chem. Soc.* **2025**, *147* (16), 14015−14023.
(31) Mahboub, M.; Maghsoudiganjeh, H.; Pham, A. M.; Huang, Z.; Tang, M. L. Triplet Energy Transfer from PbS(Se) Nanocrystals to Rubrene: the Relationship between the Upconversion Quantum Yield and Size. *Adv. Funct. Mater.* **2016**, *26* (33), 6091−6097.
(32) Huang, Z.; Simpson, D. E.; Mahboub, M.; Li, X.; Tang, M. L. Ligand Enhanced Upconversion of Near-Infrared Photons with Nanocrystal Light Absorbers. *Chem. Sci.* **2016**, *7* (7), 4101−4104.
(33) He, S.; Lai, R.; Jiang, Q.; Han, Y.; Luo, X.; Tian, Y.; Liu, X.; Wu, K. Engineering Sensitized Photon Upconversion Efficiency via Nanocrystal Wavefunction and Molecular Geometry. *Angew. Chem., Int. Ed.* **2020**, *59* (40), 17726−17731.
(34) Luo, X.; Lai, R.; Li, Y.; Han, Y.; Liang, G.; Liu, X.; Ding, T.; Wang, J.; Wu, K. Triplet Energy Transfer from $CsPbBr_3$ Nanocrystals Enabled by Quantum Confinement. *J. Am. Chem. Soc.* **2019**, *141* (10), 4186−4190.
(35) Luo, X.; Han, Y.; Chen, Z.; Li, Y.; Liang, G.; Liu, X.; Ding, T.; Nie, C.; Wang, M.; Castellano, F. N.; et al. Mechanisms of triplet energy transfer across the inorganic nanocrystal/organic molecule interface. *Nat. Commun.* **2020**, *11* (1), 28.
(36) Luo, X.; Liang, G.; Han, Y.; Li, Y.; Ding, T.; He, S.; Liu, X.; Wu, K. Triplet Energy Transfer from Perovskite Nanocrystals Mediated by Electron Transfer. *J. Am. Chem. Soc.* **2020**, *142* (25), 11270−11278.
(37) Jiang, L.-H.; Miao, X.; Zhang, M.-Y.; Li, J.-Y.; Zeng, L.; Hu, W.; Huang, L.; Pang, D.-W. Near Infrared-II Excited Triplet Fusion Upconversion with Anti-Stokes Shift Approaching the Theoretical Limit. *J. Am. Chem. Soc.* **2024**, *146* (15), 10785−10797.
(38) Xu, Z.; Huang, Z.; Li, C.; Huang, T.; Evangelista, F. A.; Tang, M. L.; Lian, T. Tuning the Quantum Dot (QD)/Mediator Interface for Optimal Efficiency of QD-Sensitized Near-Infrared-to-Visible Photon Upconversion Systems. *ACS Appl. Mater. Interfaces* **2020**, *12* (32), 36558−36567.
(39) Xu, Z.; Huang, Z.; Jin, T.; Lian, T.; Tang, M. L. Mechanistic Understanding and Rational Design of Quantum Dot/Mediator Interfaces for Efficient Photon Upconversion. *Acc. Chem. Res.* **2021**, *54* (1), 70−80.
(40) Zhang, Z.; Sung, J.; Toolan, D. T. W.; Han, S.; Pandya, R.; Weir, M. P.; Xiao, J.; Dowland, S.; Liu, M.; Ryan, A. J.; et al. Ultrafast Exciton Transport at Early Times in Quantum Dot Solids. *Nat. Mater.* **2022**, *21* (5), 533−539.
(41) Kagan, C. R.; Murray, C. B. Charge Transport in Strongly Coupled Quantum Dot Solids. *Nat. Nanotechnol.* **2015**, *10* (12), 1013−1026.
(42) You, Z.-Q.; Hsu, C.-P. Theory and Calculation for the Electronic Coupling in Excitation Energy Transfer. *Int. J. Quantum Chem.* **2014**, *114* (2), 102−115.
(43) Dexter, D. L. A Theory of Sensitized Luminescence in Solids. *J. Chem. Phys.* **1953**, *21* (5), 836−850.
(44) Biondi, M.; Choi, M.-J.; Lee, S.; Bertens, K.; Wei, M.; Kirmani, A. R.; Lee, G.; Kung, H. T.; Richter, L. J.; Hoogland, S.; et al. Control Over Ligand Exchange Reactivity in Hole Transport Layer Enables High-Efficiency Colloidal Quantum Dot Solar Cells. *ACS Energy Lett.* **2021**, *6* (2), 468−476.
(45) Weidman, M. C.; Nguyen, Q.; Smilgies, D.-M.; Tisdale, W. A. Impact of Size Dispersity, Ligand Coverage, and Ligand Length on the Structure of PbS Nanocrystal Superlattices. *Chem. Mater.* **2018**, *30* (3), 807−816.
(46) Aqoma, H.; Al Mubarok, M.; Hadmojo, W. T.; Lee, E.-H.; Kim, T.-W.; Ahn, T. K.; Oh, S.-H.; Jang, S.-Y. High-Efficiency Photovoltaic Devices using Trap-Controlled Quantum-Dot Ink prepared via Phase-Transfer Exchange. *Adv. Mater.* **2017**, *29* (19), 1605756.
(47) Dirin, D. N.; Dreyfuss, S.; Bodnarchuk, M. I.; Nedelcu, G.; Papagiorgis, P.; Itskos, G.; Kovalenko, M. V. Lead Halide Perovskites and Other Metal Halide Complexes As Inorganic Capping Ligands for Colloidal Nanocrystals. *J. Am. Chem. Soc.* **2014**, *136* (18), 6550−6553.
(48) Zhang, H.; Jang, J.; Liu, W.; Talapin, D. V. Colloidal Nanocrystals with Inorganic Halide, Pseudohalide, and Halometallate Ligands. *ACS Nano* **2014**, *8* (7), 7359−7369.
(49) Kovalenko, M. V.; Scheele, M.; Talapin, D. V. Colloidal Nanocrystals with Molecular Metal Chalcogenide Surface Ligands. *Science* **2009**, *324* (5933), 1417−1420.
(50) dos Santos, J. A. L.; Baum, F.; Kohlrausch, E. C.; Tavares, F. C.; Pretto, T.; dos Santos, F. P.; Santos, J. F. L.; Khan, S.; Santos, M. J. L. 3-Mercaptopropionic, 4-Mercaptobenzoic, and Oleic Acid-Capped CdSe Quantum Dots: Interparticle Distance, Anchoring Groups, and Surface Passivation. *J. Nanomater.* **2019**, *2019* (1), 2796746.
(51) Liu, M.; Voznyy, O.; Sabatini, R.; García de Arquer, F. P.; Munir, R.; Balawi, A. H.; Lan, X.; Fan, F.; Walters, G.; Kirmani, A. R.; et al. Hybrid Organic−Inorganic Inks Flatten the Energy Landscape in Colloidal Quantum Dot Solids. *Nat. Mater.* **2017**, *16* (2), 258−263.
(52) Weidman, M. C.; Yager, K. G.; Tisdale, W. A. Interparticle Spacing and Structural Ordering in Superlattice PbS Nanocrystal Solids Undergoing Ligand Exchange. *Chem. Mater.* **2015**, *27* (2), 474−482.
(53) Sun, R.; Zang, J.; Lai, R.; Yang, W.; Ji, B. Near-Infrared-to-Visible Photon Upconversion with Efficiency Exceeding 21% Sensitized by InAs Quantum Dots. *J. Am. Chem. Soc.* **2024**, *146* (26), 17618−17623.
(54) Miyashita, T.; Jaimes, P.; Lian, T.; Tang, M. L.; Xu, Z. Quantifying the Ligand-Induced Triplet Energy Transfer Barrier in a Quantum Dot-Based Upconversion System. *J. Phys. Chem. Lett.* **2022**, *13* (13), 3002−3007.
(55) Huang, Z.; Xu, Z.; Mahboub, M.; Li, X.; Taylor, J. W.; Harman, W. H.; Lian, T.; Tang, M. L. PbS/CdS Core−Shell Quantum Dots Suppress Charge Transfer and Enhance Triplet Transfer. *Angew. Chem., Int. Ed.* **2017**, *56* (52), 16583−16587.
(56) Huang, Z.; Xu, Z.; Mahboub, M.; Liang, Z.; Jaimes, P.; Xia, P.; Graham, K. R.; Tang, M. L.; Lian, T. Enhanced Near-Infrared-to-Visible Upconversion by Synthetic Control of PbS Nanocrystal Triplet Photosensitizers. *J. Am. Chem. Soc.* **2019**, *141* (25), 9769−9772.
(57) El-Ballouli, A. A. O.; Alarousu, E.; Bernardi, M.; Aly, S. M.; Lagrow, A. P.; Bakr, O. M.; Mohammed, O. F. Quantum Confinement-Tunable Ultrafast Charge Transfer at the PbS Quantum Dot and Phenyl-C_{61}-butyric Acid Methyl Ester Interface. *J. Am. Chem. Soc.* **2014**, *136* (19), 6952−6959.
(58) Gilmore, R. H.; Lee, E. M. Y.; Weidman, M. C.; Willard, A. P.; Tisdale, W. A. Charge Carrier Hopping Dynamics in Homogeneously Broadened PbS Quantum Dot Solids. *Nano Lett.* **2017**, *17* (2), 893−901.
(59) Albaladejo-Siguan, M.; Baird, E. C.; Becker-Koch, D.; Li, Y.; Rogach, A. L.; Vaynzof, Y. Stability of Quantum Dot Solar Cells: A Matter of (Life)Time. *Adv. Energy Mater.* **2021**, *11* (12), 2003457.
(60) Zheng, B.; Zhong, D.; Xie, T.; Zhou, J.; Li, W.; Ilyas, A.; Lu, Y.; Zhou, M.; Deng, R. Near-Infrared Photosensitization via Direct Triplet Energy Transfer from Lanthanide Nanoparticles. *Chem* **2021**, *7* (6), 1615−1625.
(61) Han, S.; Deng, R.; Gu, Q.; Ni, L.; Huynh, U.; Zhang, J.; Yi, Z.; Zhao, B.; Tamura, H.; Pershin, A.; et al. Lanthanide-Doped Inorganic Nanoparticles Turn Molecular Triplet Excitons Bright. *Nature* **2020**, *587* (7835), 594−599.
(62) Li, X.; Fast, A.; Huang, Z.; Fishman, D. A.; Tang, M. L. Complementary Lock-and-Key Ligand Binding of a Triplet Transmitter to a Nanocrystal Photosensitizer. *Angew. Chem., Int. Ed.* **2017**, *56* (20), 5598−5602.
(63) Piland, G. B.; Huang, Z.; Lee Tang, M.; Bardeen, C. J. Dynamics of Energy Transfer from CdSe Nanocrystals to Triplet

https://doi.org/10.1021/acsnano.5c22144
ACS Nano XXXX, XXX, XXX−XXX

States of Anthracene Ligand Molecules. *J. Phys. Chem. C* **2016**, *120* (11), 5883−5889.
(64) VanOrman, Z. A.; Weiss, R.; Bieber, A. S.; Chen, B.; Nienhaus, L. Mechanistic Insight into CdSe Nanoplatelet-Sensitized Upconversion: Size and Stacking Induced Effects. *Chem. Commun.* **2023**, *59* (3), 322−325.
(65) Hasham, M.; Narayanan, P.; Yarur Villanueva, F.; Green, P. B.; Imperiale, C. J.; Wilson, M. W. B. Sequential Carrier Transfer Can Accelerate Triplet Energy Transfer from Functionalized CdSe Nanocrystals. *J. Phys. Chem. Lett.* **2023**, *14* (7), 1899−1909.
(66) Garakyaraghi, S.; Mongin, C.; Granger, D. B.; Anthony, J. E.; Castellano, F. N. Delayed Molecular Triplet Generation from Energized Lead Sulfide Quantum Dots. *J. Phys. Chem. Lett.* **2017**, *8* (7), 1458−1463.
(67) Mi, Z.; Bian, H.; Yang, C.; Dou, Y.; Bettiol, A. A.; Liu, X. Real-Time Single-Proton Counting with Transmissive Perovskite Nanocrystal Scintillators. *Nat. Mater.* **2024**, *23* (6), 803−809.
(68) Arima, D.; Hidaka, S.; Yokomori, S.; Niihori, Y.; Negishi, Y.; Oyaizu, R.; Yoshinami, T.; Kobayashi, K.; Mitsui, M. Triplet-Mediator Ligand-Protected Metal Nanocluster Sensitizers for Photon Upconversion. *J. Am. Chem. Soc.* **2024**, *146* (24), 16630−16638.
(69) Arima, D.; Mitsui, M. Structurally Flexible Au−Cu Alloy Nanoclusters Enabling Efficient Triplet Sensitization and Photon Upconversion. *J. Am. Chem. Soc.* **2023**, *145* (12), 6994−7004.
(70) Yu, W. W.; Falkner, J. C.; Shih, B. S.; Colvin, V. L. Preparation and Characterization of Monodisperse PbSe Semiconductor Nanocrystals in a Noncoordinating Solvent. *Chem. Mater.* **2004**, *16* (17), 3318−3322.
(71) Nordell, K. J.; Boatman, E. M.; Lisensky, G. C. A Safer, Easier, Faster Synthesis for CdSe Quantum Dot Nanocrystals. *J. Chem. Educ.* **2005**, *82* (11), 1697.
(72) Müller, A. M.; Avlasevich, Y. S.; Schoeller, W. W.; Müllen, K.; Bardeen, C. J. Exciton Fission and Fusion in Bis(tetracene) Molecules with Different Covalent Linker Structures. *J. Am. Chem. Soc.* **2007**, *129* (46), 14240−14250.
(73) Okamoto, T.; Suzuki, T.; Tanaka, H.; Hashizume, D.; Matsuo, Y. Tetracene Dicarboxylic Imide and Its Disulfide: Synthesis of Ambipolar Organic Semiconductors for Organic Photovoltaic Cells. *Chem. - Asian J.* **2012**, *7* (1), 105−111.
(74) Wang, F.; Deng, R.; Liu, X. Preparation of Core-shell $NaGdF_4$ Nanoparticles Doped with Luminescent Lanthanide Ions to be Used as Upconversion-Based Probes. *Nat. Protoc.* **2014**, *9* (7), 1634−1644.
(75) Abraham, M. J.; Murtola, T.; Schulz, R.; Páll, S.; Smith, J. C.; Hess, B.; Lindahl, E. GROMACS: High Performance Molecular Simulations through Multi-level Parallelism from Laptops to Supercomputers. *SoftwareX* **2015**, *1−2*, 19−25.
(76) Wang, J.; Wolf, R. M.; Caldwell, J. W.; Kollman, P. A.; Case, D. A. Development and Testing of a General Amber Force Field. *J. Comput. Chem.* **2004**, *25* (9), 1157−1174.
(77) Rappe, A. K.; Casewit, C. J.; Colwell, K. S.; Goddard, W. A., III; Skiff, W. M. UFF, a full periodic table force field for molecular mechanics and molecular dynamics simulations. *J. Am. Chem. Soc.* **1992**, *114* (25), 10024−10035.
(78) Bussi, G.; Donadio, D.; Parrinello, M. Canonical Sampling through Velocity Rescaling. *J. Chem. Phys.* **2007**, *126* (1), 014101.
(79) Hess, B.; Bekker, H.; Berendsen, H. J. C.; Fraaije, J. G. E. M. LINCS: A Linear Constraint Solver for Molecular Simulations. *J. Comput. Chem.* **1997**, *18* (12), 1463−1472.

https://doi.org/10.1021/acsnano.5c22144
ACS Nano XXXX, XXX, XXX−XXX